CAPTURE CROSS SECTIONS IN THE KEV REGION

by

Wayne Wesley Campbell

Thesis submitted to the Graduate Faculty of the

Virginia Polytechnic Institute

in partial fulfillment of the requirements for the degree of

DOCTOR OF PHILOSOPHY

in

Physics

APPROVED:

Chairman Dr. A. K. Furr

Dr. James A. Jacobs

Dr. A. Robeson

Dr. R. L. Bowden

Dr. R. F. Tipsword

October 1969

Blacksburg, Virginia

ACKNOWLEDGEMENTS

To Dr. A. Keith Furr, the author's thesis advisor, goes a very special appreciation for his patience, faith, and constant encouragement. His many suggestions during both the project and the writing of this dissertation, as well as the careful attention which he gave to the review, have made him invaluable to the author. Gratitude is also extended to Drs. James A. Jacobs, Andrew Robeson, Ray F. Tipsword, and Robert L. Bowden, all of the V.P.I. Physics Department, for serving on the author's committee.

To Dr. Ron Onega and the low-energy nuclear group, the author would like to express sincere thanks for the thoughtful attention which was always given to his many questions and problems.

The author would like to acknowledge

and for their many helpful discussions during this project.

To his wife, the author wishes to express warmest appreciation for her encouragement, understanding, and patience offered throughout his academic career.

Finally, the author wishes to acknowledge the Atomic Energy Commission which provided financial assistance in the form of a Traineeship under which part of this work was performed.

TABLE OF CONTENTS

LIST OF FIGURES

LIST OF TABLES

INTRODUCTION

The advent of fast reactors has made it imperative to study neutron cross sections at epithermal energies[1]. Definitive values for these cross sections and the nuclear resonance parameters which can be derived from them also greatly enhance studies of stellar evolution and the optical model theory of the nucleus[2,3]. The above exigencies have caused vast amounts of data to be generated in this field. Nevertheless, gaps do exist and some data are very poor, leaving extensive work yet to be done. For example, the latest edition of Neutron Cross Sections[23], the "Barn Book", gives values for the capture cross section of natural silver with error bars of ± 40%. Values for average resonance parameters are even more inconsistent from one experimenter to another as can be seen in Table[III], page[67].

Neutron cross sections are generally examined by one of several ways, among which are

(a) time-of-flight method using a linear accelerator[31,32],

(b) spherical shell transmission[4,33],

(c) time-of-flight method using a pulsed Van de Graaff[8,9,10],

(d) slowing-down-time spectrometer[34,35],

(e) time-of-flight method using a reactor and beam chopper[11],

(f) using the monoenergetic beam of neutrons available at back angles to a neutron producing target placed in the beam of a steady current Van de Graaff[12,13],

(g) boron filter techniques[5,6,7].

No single method is best for the entire energy range of from several eV to several hundred keV where data are needed; however, each one has

intrinsic advantages over the others in specific cases. These advantages along with some disadvantages are described quite well in a review by Gibbons[14]. The work now being done at V.P.I. in this field involves methods (f) and (g) above, using the V.P.I. research reactor and the 4 mV Van de Graaff accelerator. These two techniques differ radically but both involve activation of similar samples which are counted with a common detector system. Hopefully, systematic errors in each technique will differ with each method and can be eliminated between the two measurements.

The experiment described in this work employs the technique of activating a sample with $^{7}Li(p,n)^{7}Be$ neutrons and counting the resulting induced activity in a separate lab; therefore, the method is dependent upon the sample having a suitable neutron cross section for production of at least one radioactive isotope with a half life long enough to make transfer feasible and short enough to make activation times reasonable. Although this limits the number of isotopes which can be studied, the procedures are straightforward, and for these isotopes it is perhaps the best method in the 1 to 200 keV energy region.

Neutron capture cross sections and average resonance parameters have been determined in the present work for 3 keV $\leq E_n \leq$ 155 keV. For medium and heavy nuclei, not close to closed shells this energy region involves contributions of many resonances. In addition, over this restricted energy it may be assumed that only s-, p-, and to a much less degree, d-wave neutrons contribute to the neutron capture cross sections[13].

The technique has been employed in the present work to study ^{127}I, ^{115}In, ^{107}Ag, ^{109}Ag, and natural Ag. All cross sections were normalized to thermal cross sections and the ^{127}I cross section at 24 keV. The results, given in Section (VII), are in general good agreement with those of other workers although, as noted in the introductory paragraph, there are often wide variations in these other data.

EXPERIMENTAL PROCEDURE

A. Sample Preparation

As mentioned in the introduction the isotopes ^{115}In, ^{127}I, ^{107}Ag, ^{109}Ag, and natural silver were studied in this work. In each case the samples were made into an annular form having a width of 4 mm, a diameter of 72 mm for the annulus, with the thickness varying with each element.

Indium wire of 1.58 mm diameter was rolled in a hand operated rolling mill to a thickness of 0.15 mm, equivalent to an areal density of 111.0 mg/cm^2. The silver samples were made by folding 0.013 mm foil into eight thicknesses, making a total thickness of 0.1 mm, with an areal density of 105.0 mg/cm^2. The iodine, not being a metal, was obtained in the form of KI crystals. These crystals were crushed to a fine powder and mixed with distilled water to form a thick slurry. The resulting mixture was then painted onto a steel supporting ring of 0.25 mm thickness and dried. The resultant KI shell was about 1.0 mm thick with the areal density of iodine being approximately 200 mg/cm^2. No appreciable activity was obtained from the steel ring or from the potassium. The samples were kept thin enough so that self-shielding corrections were not necessary since the greatest neutron attentuation (for the KI mixture) was less than 0.5%.

All samples were activated by being affixed to the same steel support rings used to support the KI slurry. The ring with sample attached was supported by a plexiglass ring as illustrated in Fig. 1. This plexiglass ring served several purposes. Not only did it

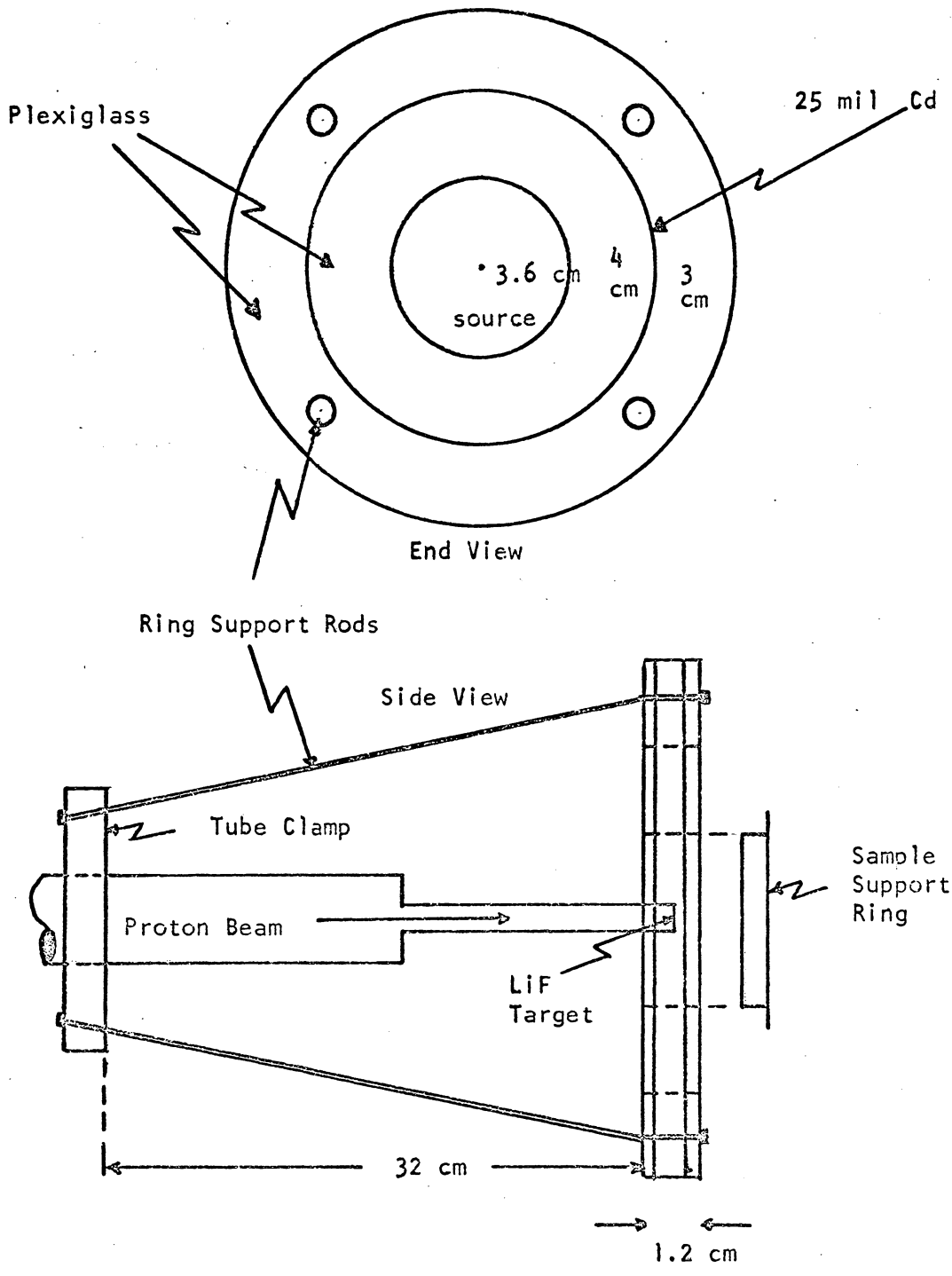

Sample Holder

FIGURE 1

retain the sample, but it partially shielded the sample from room scattered neutrons and helped to shield the neutron monitor from a direct neutron beam. This last point will be discussed in the next section. Measurements made with a small monitor showed that a negligibly small number of multiply scattered neutrons from the support returned to the sample and activated it.

B. Sample Activation and Neutron Monitoring

Neutrons are produced by the $^{7}Li(p,n)^{7}Be$ reaction which has been studied in great detail[15,16,17,18] and whose characteristics are well known. The threshold of this reaction is 1.8811 meV, at which energy neutrons of 29 keV are emitted in a narrow forward cone. As the proton energy is increased the cone spreads and the neutron energy increases until, at E_p = 1.9255 meV, neutrons are being produced at an angle of 90^{o} with E_n = 3 keV. As E_p increases, E_n increases and the neutron beam is monoenergetic. At higher proton energies than were used here, additional neutron groups are produced by the reaction[16].

The neutron producing targets used in this experiment were made by evaporating LiF powder onto 0.25 mm tantalum in an evacuated chamber. Targets of this type are discussed by Gibbons, et al[16]. Two different targets were used; one which was 1.7 keV thick for ^{115}In and one of 1.9 keV thickness for all other samples and for the normalizing run taken at the end of the measurements. Thicknesses were determined by the method outlined below described by Gibbons in the reference just cited.

A paraffin covered $^{10}BF_3$ detector was placed at an angle of 0° to the proton beam and the proton beam on the target was adjusted to well below the (p,n) threshold of 1.8811 meV. Small increments were made in the proton energy with corresponding neutron counts being recorded. This was continued until the neutron yield reached a maximum and began to decrease. A graph was made of the relative yield at 0° versus proton energy. The thickness was determined by extrapolating the linear portion of the curve down to zero and up to the value of the maximum and calling the target thickness the energy difference between these two intersections.

It was also necessary to determine the (p,n) threshold for a proton of average energy which has penetrated half the LiF target. By defining the threshold in this manner the neutron energy spread would be symmetric about the nominal energy. The threshold as defined above was then taken to be the energy corresponding to the maximum value of the neutron yield. Figure (2) shows the neutron counts at 0° versus proton energy curve from which the thickness and threshold were determined for the 1.9 keV thick target.

One further point deserves comment at this time. At 0° the spread in neutron energy is nearly equal to the spread in proton energy, but at greater angles this is not true. The expression for the ratio of neutron energy spread to proton energy spread for ^7Li at a lab angle ψ is given by (16)

$$\left.\frac{\Delta E_n}{\Delta E_p}\right|_\psi = \frac{\cos\psi + Z}{64}\left[\cos\psi + Z + \frac{49\ E_{th}}{Z\ E_p}\right] \qquad (1)$$

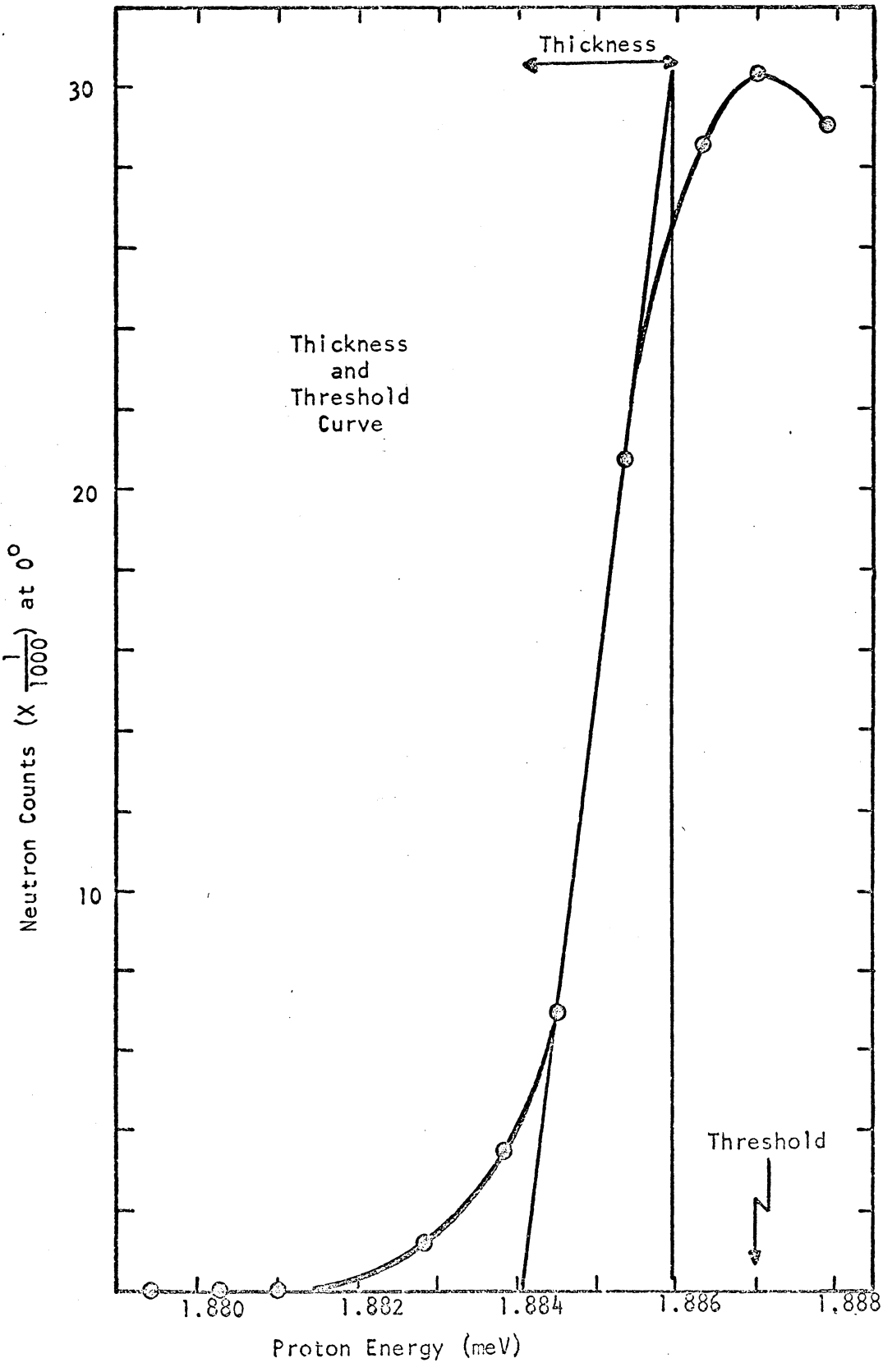
Thickness
30
Thickness
and
Threshold
Curve
20
Neutron Counts (X $\frac{1}{1000}$) at 0°
10
Threshold
1.880
1.882
1.884
1.886
1.888
Proton Energy (meV)

FIGURE 2

where

E_{th} = energy of the threshold

$Z^2 = [49(E_p - E_{th})/E_p] - \sin^2 \psi$.

Thus the spread in neutron energy at an angle of 90° is only three fourths the proton energy spread.

The samples used in this work were placed at an angle of 90° to the proton beam to take advantage of the monoenergetic property of the lithium (p,n) yield at angles $\geq 90^\circ$ and still have the greatest possible flux. The geometry of the sample placed in this position was such that it subtended a half-angle of 3° 11' to the neutron source. This resulted in an energy resolution, due to geometry alone, of approximately 4% for E_n = 155 keV, increasing to about 40% at E_n = 3 keV. This can best be seen looking at Fig. (3). Better resolution is available at greater back angles but the neutron yield decreases, so that one trades poorer energy resolution for poorer counting statistics.

Irradiation times varied from 7.5 minutes for silver to 30 minutes for indium, determined partially by whether good counting statistics were obtained, and partially by the half life of the target. Two similar samples of each element were made to enable the experimenter to count one sample while the other was being activated. This procedure was then repeated, alternating the samples such that each sample was irradiated at each energy. The two activities were added together, after necessary corrections and normalizations, to prevent errors from arising due to the differences in the samples.

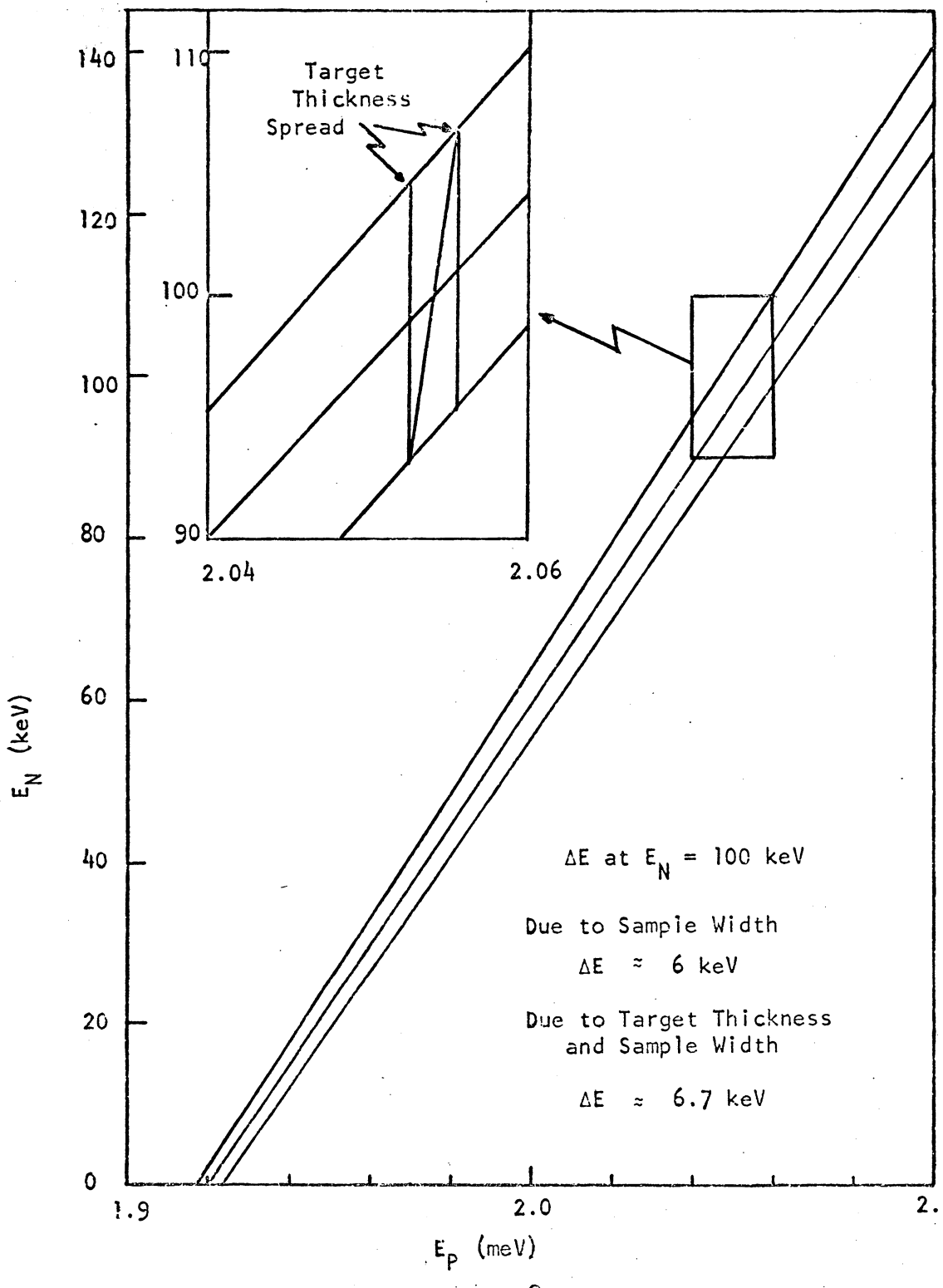

Energy Spread at 90°

FIGURE 3

The activity of a sample irradiated for a time, t, is given by

$$A = N\sigma\phi(1 - e^{-\lambda t}) \tag{2}$$

where

N = number of target atoms present

σ = cross section of target

ϕ = neutron flux

λ = decay constant = ln 2/(half life)

t = activation time

Obviously, from this equation it is necessary that one know the relative flux at each activation energy if a cross section versus energy curve is to be made.

If the neutron flux were constant throughout a single activation and the activation times were also constant, the cross section at energy E_2 relative to that at E_1 could be given by the simple relation

$$\sigma(E_2) = \sigma(E_1) \frac{A(E_2)}{A(E_1)} \frac{\phi(E_1)}{\phi(E_2)} \tag{3}$$

However, a constant flux is not the usual case with a Van de Graaff. Therefore one must make a correction for this effect. By recording a neutron counting rate, F_i, during the activation period, at intervals of time that are short compared to the half life of the radioactive product, it is possible to write down the equation

$$F = \sum_i F_i e^{-\lambda t_i} \tag{4}$$

where

λ = decay constant

t_i = time from i^{th} interval to end of activation.

Equation 4 gives the effective neutron counts which, if all neutrons had been formed at a constant rate during the last time interval, would have resulted in the observed activity (i.e. corrects for both a variable flux and radioactive decay during activation).

A block diagram of the neutron monitoring system is given in Fig. (4). The multi-channel analyzer was used in the multiscale mode whereby all neutron counts arriving in a certain time interval were stored in a certain channel, regardless of their energies. By monitoring in this manner, one can make use of Eq. 4 to correct for variations in neutron flux during the period of activation.

During a survey of the literature in the field it was found that a neutron source located in a "vault" such as the target area of the Van de Graaff room gave rise to a large number of room scattered neutrons to add to the neutron background[19]. Extensive data were taken by the author to determine the magnitude of this correction factor using a small, silicon, surface barrier detector operated at room temperature. This detector was covered with a thin ^{10}B disc which served to produce detectable ions by the $^{10}B(n,\alpha)^{7}Li$ reaction. A survey of the target area was taken recording neutron counts versus distance from the source, keeping the neutron energy constant. It was hoped that it would be possible to thereby separate the room background and foreground (direct neutrons from the source), assuming a $1/r^2$ dependence for the foreground. A sample of this survey is

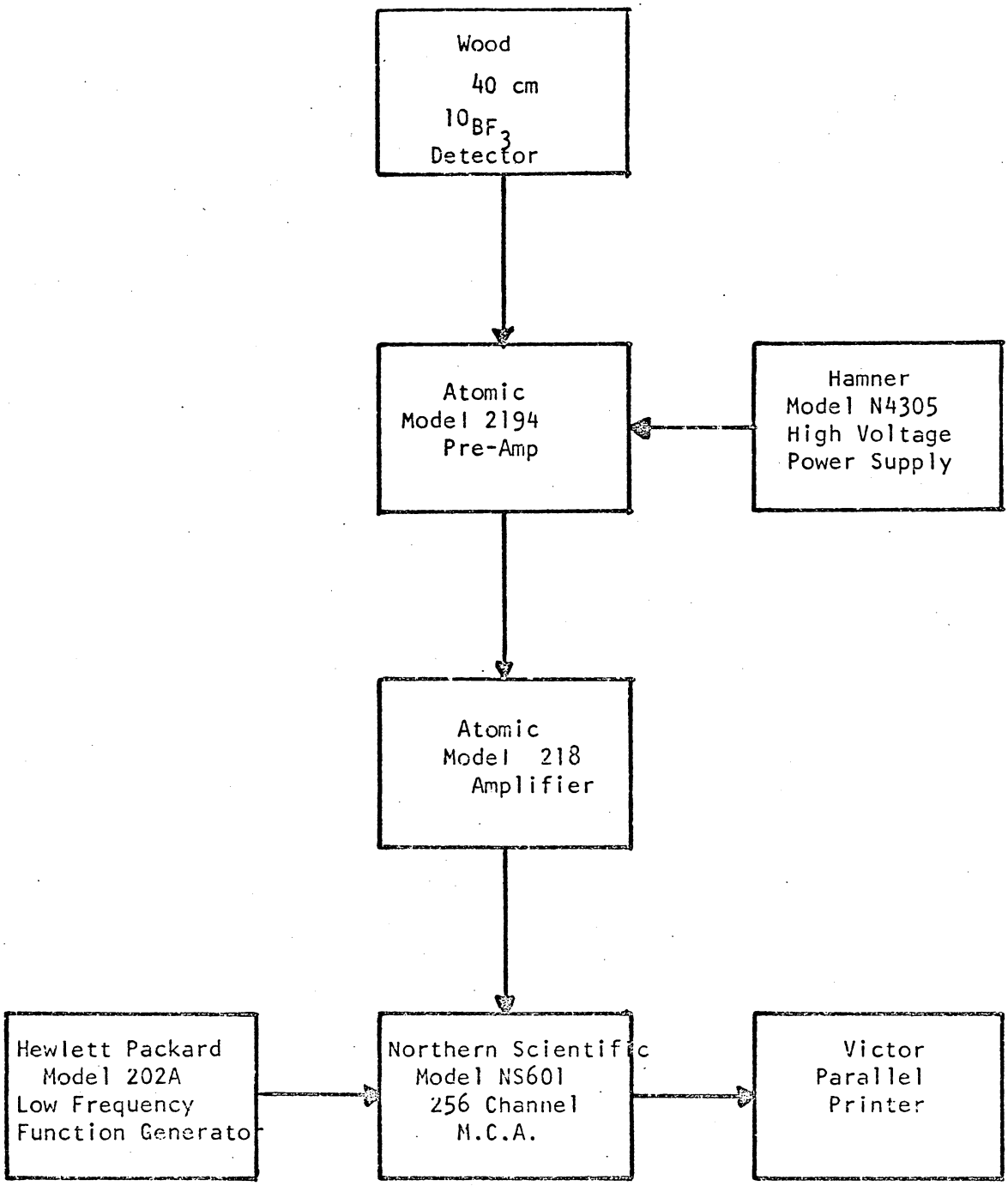

Block Diagram of Neutron Monitoring System

FIGURE 4

given in Fig. (5) for a neutron energy, at 90^{o} to the proton beam, of 43 keV. Background counts resulting from natural radiation, electronic noise, and Van de Graaff related radiation have been subtracted from these data.

The open circles of Fig. (5) represent the corrected neutron counts and the closed circles represent the resultant after subtracting a background of 5000 counts from each point. This background was arrived at by trial and error. The straight line represents a $1/r^2$ curve and strengthens the assumption of such a dependence. The variance of the closed circles from the $1/r^2$ curve at short distances can be attributed to the inability to locate the exact position of the proton beam on the lithium target (i.e. position of the neutron source). This position was uncertain to several millimeters and would result in such an error near the source, with little effect at large distances.

It was also noted from this survey that at 3.6 cm, the sample distance from the source (see Fig. 1), that the scattered background was about 6%; but at a distance of 10 cm, the closest in the same plane as the target specimen that the neutron monitor could be placed, the background was 33%. Because of this source of possible large errors it was decided that the liability of a high background from the room could be turned into an asset. By placing the detector at an angle of 90^{o} to the proton beam and behind a "shadow shield" one could then monitor the ambient neutron flux in the room and obtain results which would reflect variations in the neutron yield of the target. The monitor geometry of Fig. (6) shows the final

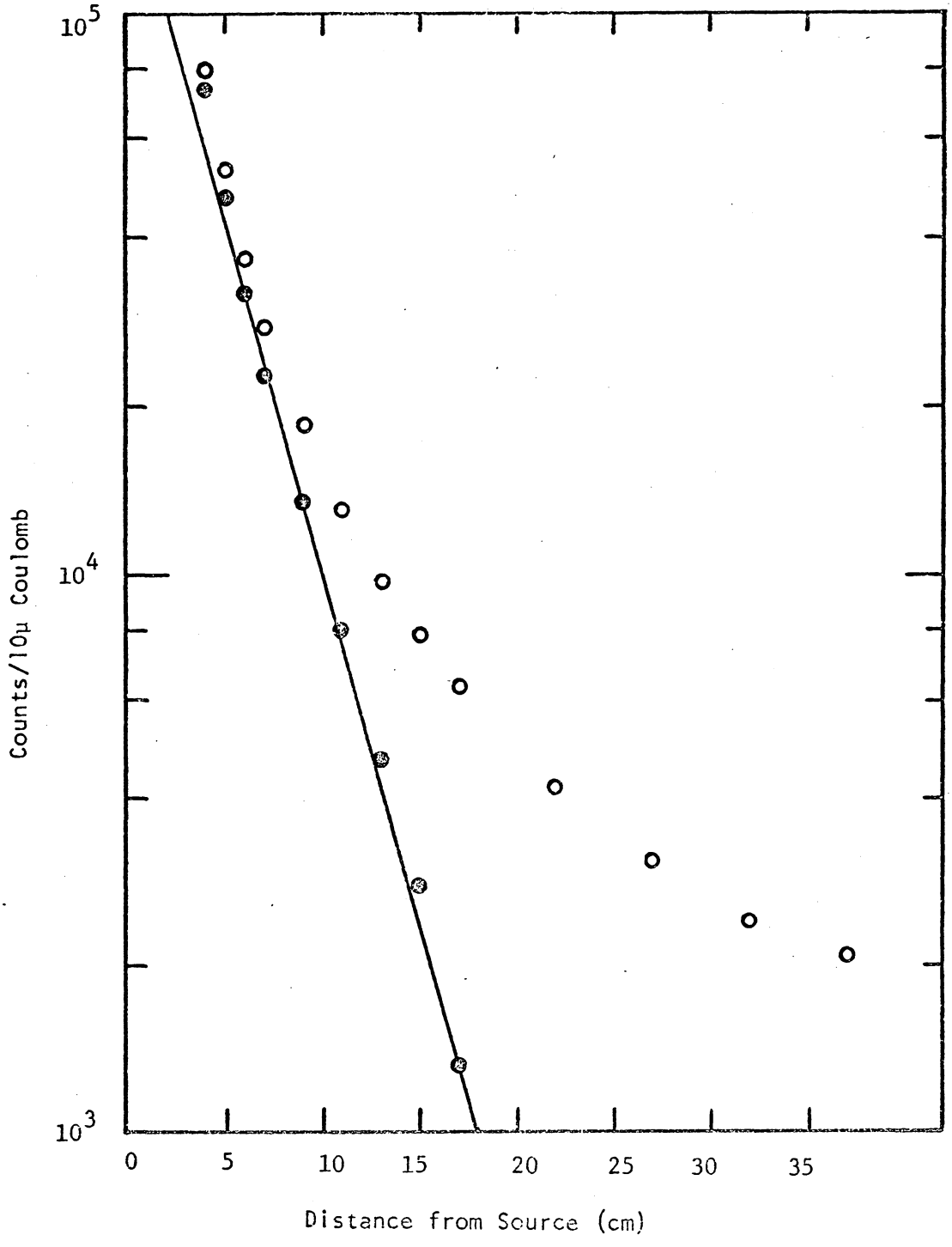

$1/r^2$ Survey

FIGURE 5

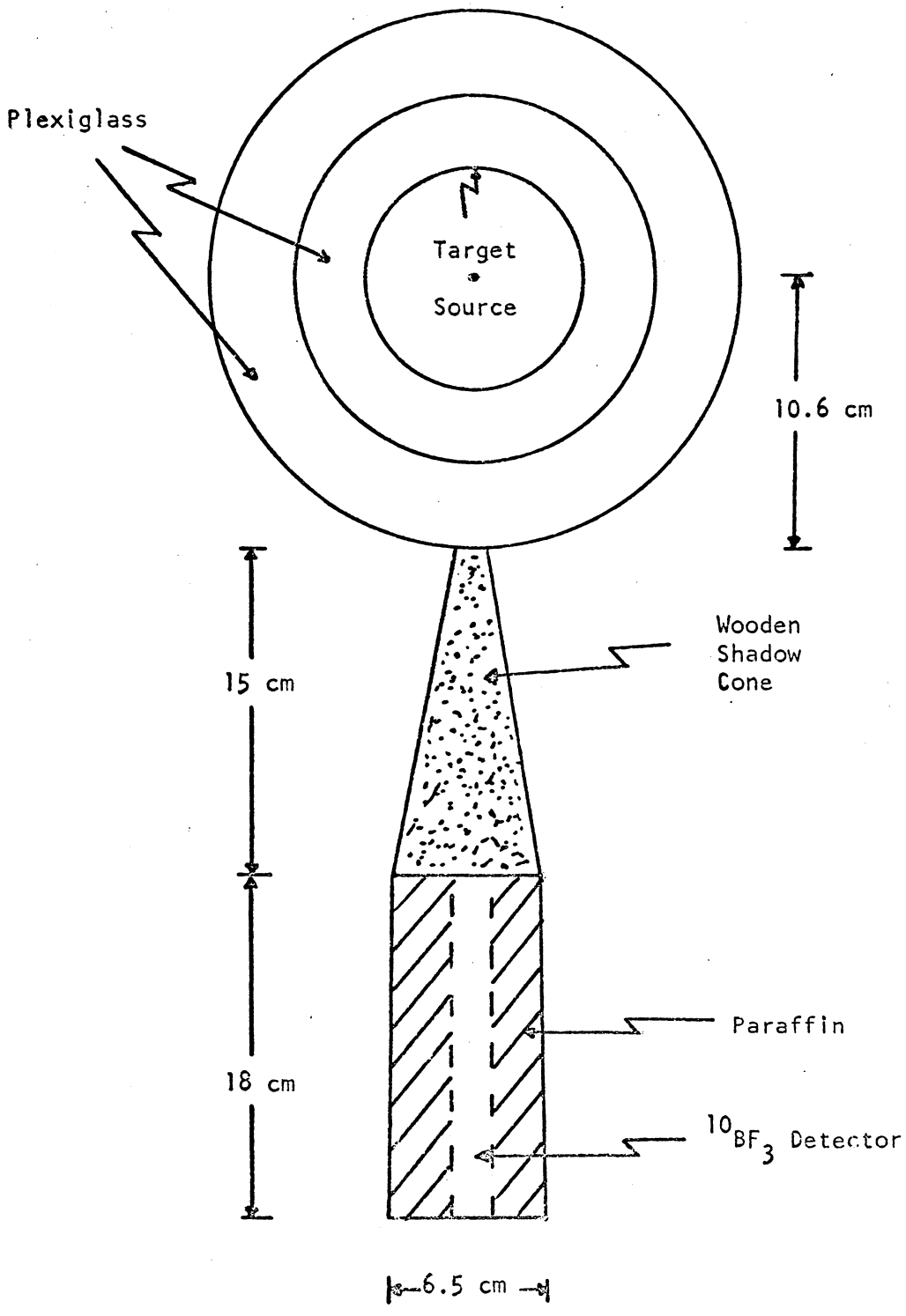

Neutron Detector

FIGURE 6

experimental setup. As stated earlier, the plexiglass ring with cadmium insert served to reduce the background at the sample and to shield the monitor from direct neutrons.

All that remained was to determine the energy dependence of the monitor detector, including variations in the number of room neutrons with proton energy (and hence neutron energy). With the setup as shown in Fig. (6) a survey was made recording the neutron monitor counts over the entire energy range from 3 to 155 keV, keeping the integrated proton current constant. The results are shown in Fig. (7) and give a monitor correction to be applied to the data. Finally, it was necessary to determine how the yield of the $^{7}Li(p,n)^{7}Be$ reaction varied with energy at 90^{o} to the proton beam. This yield correction was determined by placing the aforementioned silicon detector at a distance of 3.6 cm from the source and running a counts versus energy experiment, the results of which are shown in Fig. (8). The counts plotted in this figure have been corrected for background effects and for the 1/v dependence of the boron cross section. The details of the various corrections will be discussed in the section on analysis.

C. Counting Procedure

In order that the counting background might be as small as possible, all samples were removed from the Van de Graaff target room and carried to the counting laboratory. This lab is removed from the target room by some 25 meters and is shielded from Van de Graaff related background by several feet of concrete. A low background counting facility constructed and described by Winters[21]

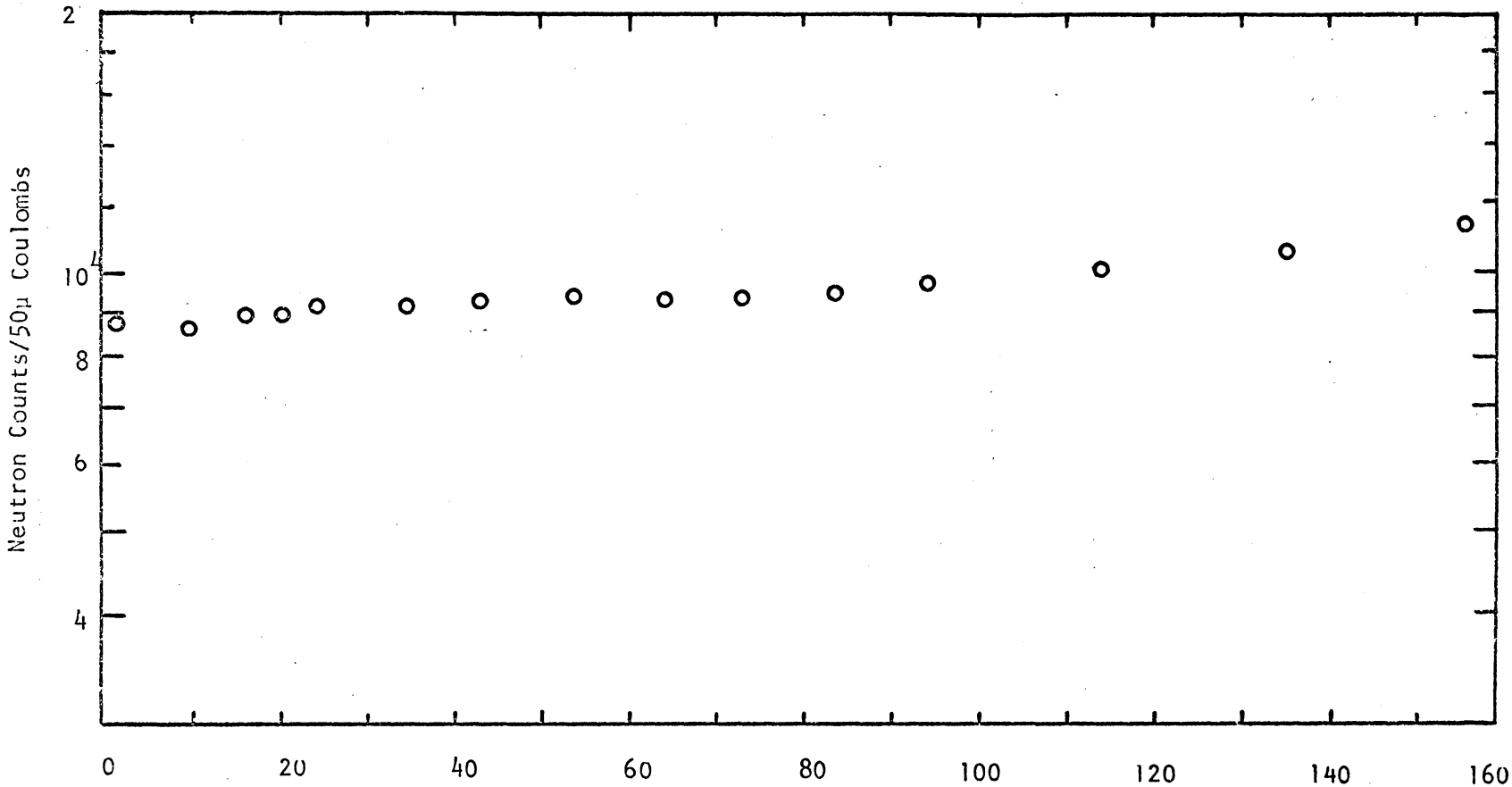

$^{10}BF_3$ Monitor Curve

FIGURE 7

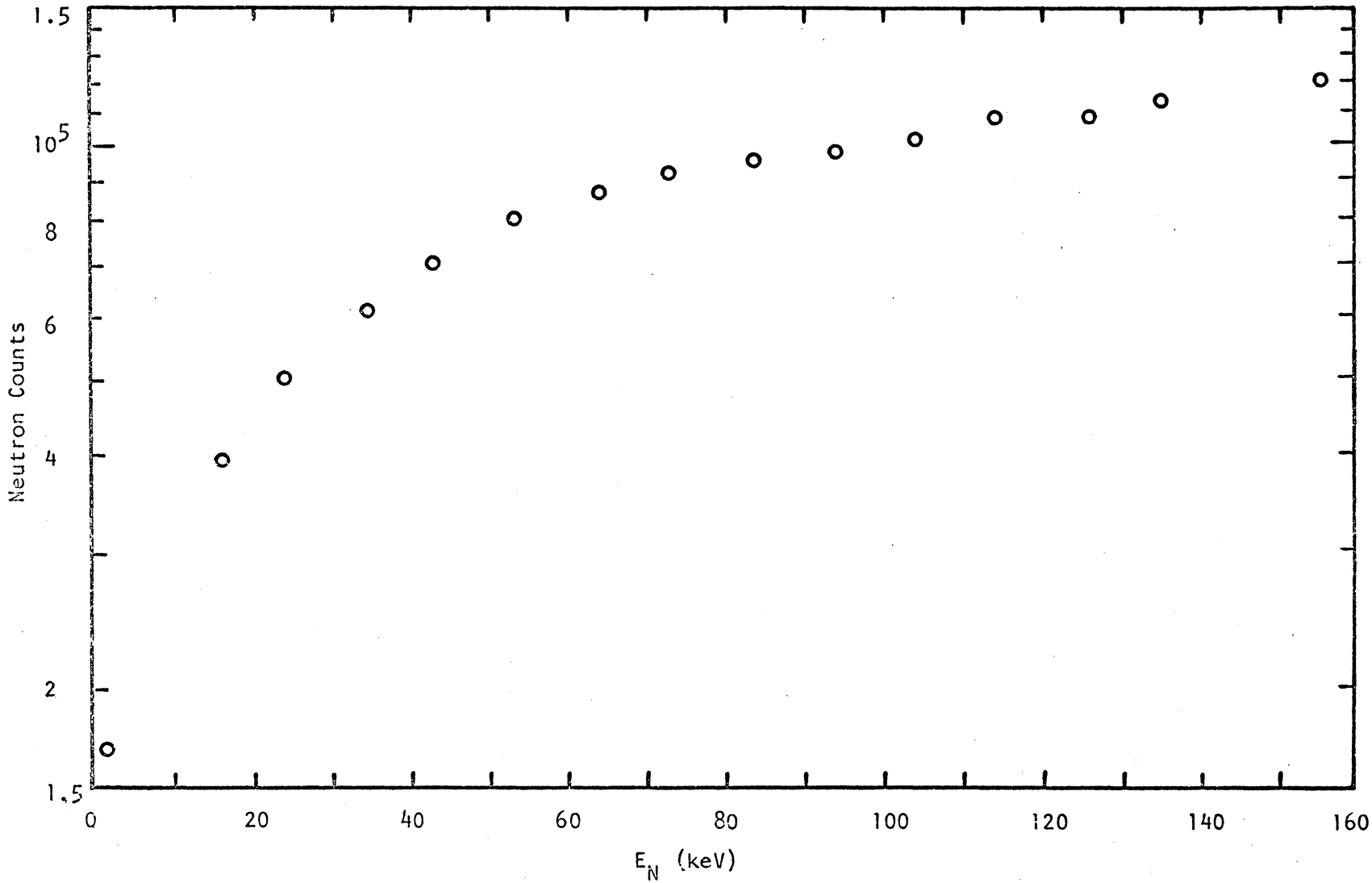

Target Yield Curve

FIGURE 8

is provided in this lab. Figure (9) is a block diagram of the counting system used in this experiment.

Several different detector assemblies were used to measure the activities of the isotopes studied. Early in the work a 7.62 X 7.62 cm NaI(Tl) detector was used. Low counting rates were obtained and a 2.54 X 12.70 cm NE102 plastic scintillator was tried since this would respond to both β and γ radiation from the sample. This improved the count rate so a well-type plastic scintillator was constructed by cutting a 3 mm wide by 5 mm deep groove in the face of a 2.54 X 10.16 cm scintillating plastic cylinder to accept the annular samples. The surface was then covered with aluminum foil to prevent light leakage. This detector proved to be the most efficient for our work.

A Cosmic Spectrastat high voltage power supply was used to power the photomultiplier for the NaI crystal, and an Atomic Model 312 high voltage power supply was used when either of the beta crystals was used. Pulses from the P-M tube were sent to a Tennelec Model TC200 amplifier and then into the multi-channel analyzer which was operated in a multi-scale mode. This mode of operation was chosen rather than a pulse height analysis mode to permit separation or identification of the radiation by the rate of decay and because the plastic scintillator used offered little hope of identification of the radiation present from the spectrum details available.

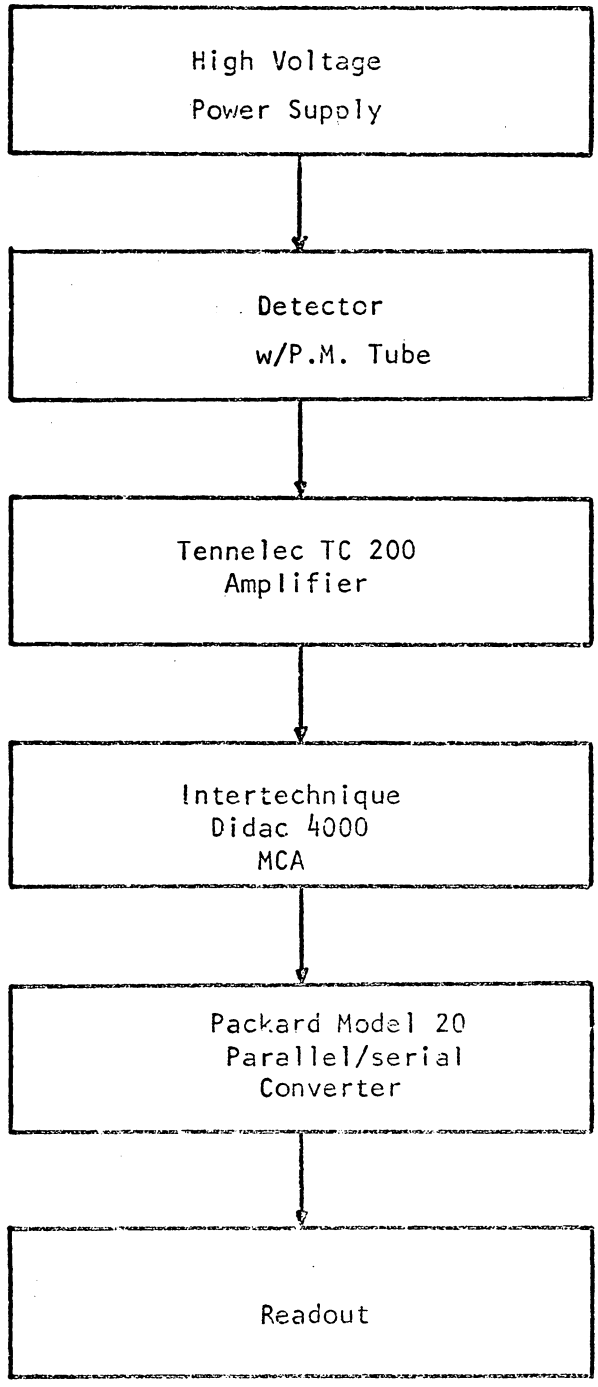

Block Diagram of β/γ Counting System

FIGURE 9

ANALYSIS

A. Cross Sections

The first quantity obtained from the activation data was the neutron cross section for capture. Several correction factors must be applied to the data but the calculation is straightforward. In general, the measured activity of a sample containing N target atoms placed in a neutron flux, $\phi(E)$, for a time, t_a, and counted for a time, t_c, is given by

$$C(E) = \varepsilon N \sigma(E) \phi(E) (1 - e^{-\lambda t_a})(e^{-\lambda t_w})(1 - e^{-\lambda t_e}) \qquad (1)$$

where

ε = counting efficiency

$\sigma(E)$ = neutron capture cross section

t_w = time between activation and counting

λ = decay constant

The efficiency, ε, of the counting system is dependent upon the geometry of both the sample and detector, as well as intrinsic characteristics of the detector. This parameter is quite difficult to obtain accurately for complex geometries so it was decided to obtain relative cross sections (i.e. an energy versus cross section curve which is identical in shape to an absolute cross section curve) for each isotope. To obtain absolute cross sections it was necessary to obtain the "exact or absolute" cross section at any one energy and then normalize the relative curve to this value. This normalization is discussed later.

By recording the various times involved during each activation and counting period, one can obtain relative cross sections by use of the equation

$$\sigma_R(E) = C(E)/\phi_R(E)F(\lambda,t_i) \qquad (2)$$

where

$C(E)$ = measured activity of the sample

$\phi_R(E)$ = relative neutron flux

$F(\lambda,t_i)$ = exponential terms in Eq. 1

It should be reemphasized that, in this discussion, relative cross section refers to the curve giving the cross section at one energy relative to that at a different energy. This is not in accord with the usual definition of relative cross section as the cross section of one isotope relative to that of another. Insertion of Eq. 2 into (1) yields

$$\sigma_R(E) = \varepsilon N \left\{\frac{\phi(E)}{\phi_R(E)}\right\} \sigma(E) \qquad (3)$$

Therefore, the constant of proportionality between relative and absolute cross sections is the product of the total efficiency, the number of target atoms in the sample, and the ratio of relative flux to absolute flux. Equation 2, in a modified form due to several correction factors outlined below, was used for the data collected in this project.

Flux Monitoring Corrections. -- There were three correction factors which had to be applied to the neutron monitor data. These are: (1) M_c, due to variations in the neutron detection efficiency with

energy, (2) Y_c, due to variations in the yield of the $^{7}Li(p,n)^{7}Be$ reaction with energy, and (3) N_c, due to variations in the neutron flux due to target evaporation and inconsistencies in the integrated proton current.

The monitor used to detect neutrons, as stated earlier, was a $^{10}BF_3$ detector. This was an ionization chamber containing boron trifluoride gas which detects neutrons by the $^{10}B(n,\alpha)^{7}Li$ reaction. The alpha particle and lithium ion produce the necessary ionization for detection. Boron-10 has a 1/v cross section, i.e. the cross section varies as $1/\sqrt{E}$, for neutrons; therefore, it is not a good detector for fast neutrons. This necessitated covering the detector with paraffin which slowed the neutron down for more efficient detection. Because we were monitoring the ambient neutron flux of the target area, it was necessary to take into account changes in this neutron "cloud" with energy. The data shown in Fig. (7), Section (V) is a result of a survey of neutrons detected versus energy. This data was taken in a short period of time so that target burnup was assumed negligible. The integrated proton current (total number of protons which struck the lithium target) was held constant so the data should reflect both the change in ambient flux as a function of energy and the detector efficiency changes with energy. The monitor correction factor, M_c, was then taken from the graph of Fig. (7) as the ratio of neutrons counted at E_i to neutrons counted at E = 155 keV.

The actual neutron yield of the n + ^{7}Li reaction varies radically with energy as can be seen in Fig. (8). This required a

correction to simulate a constant yield. The section on Experimental Procedure describes an experiment performed to obtain this yield versus energy curve which is illustrated by Fig. (8). Note that the ordinate has been corrected for background and for the 1/v dependence of the boron. Figure (8) reflects actual changes in the neutron yield with energy. The correction factor, Y_c, was taken from this graph as a ratio of neutrons counted at 155 keV to those counted at E_i.

Finally, target evaporation and integrated current changes were taken into account. Evaporation of the target is a result of the literal boiling away of the LiF by the proton beam. This can be virtually eliminated by an air-water spray directed onto the target as a coolant. However, this would have contaminated our samples (and dissolved the KI mixture) and was not used. It was found that by running the Van de Graaff with a proton current in the range of from 2 to 3 microamps target evaporation could be kept within tolerable limits and the neutron yield was also acceptable. All reasonable care was taken to provide a constant current in this range. Nevertheless changes did occur and were accounted for by forming the ratio of neutron counts at 155 keV to those at E_i. This constituted the factor N_c.

All correction factors for E_n = 155 keV were taken to be unity and succeeding factors were measured relative to this. The net result of these three corrections is given by

$$\sigma_R(E) = \frac{C(E)M_c(E)Y_c(E)N_c(E)}{F(\lambda,t_i)} \qquad (4)$$

where

M_c = monitor correction ($M_c \leq 1$)

Y_c = yield correction ($Y_c \geq 1$)

N_c = neutron correction.

Equation 4 was used in this form for each different neutron energy and yielded a curve that was directly proportional to the absolute cross section curve.

Normalization. -- Each sample was activated and counted at discrete energy intervals over the range of 3 to 155 keV. To obtain absolute cross sections the cross section of ^{127}I at 24 keV was chosen as the standard. The value used was $0.832 \pm .026$ barns as determined by Robertson[22] using the spherical shell transmission method. Iodine was then normalized to this value. For indium and silver, normalization was performed using the cross section of iodine measured in the present experiment at 24 keV and the thermal cross sections of the individual isotopes.

Consider the following ratio.

$$R = A_{th}/A_E \qquad (5)$$

where the subscripts refer to activation at thermal energy and at another energy, E.

$$\therefore \quad R = \frac{N_{th}\sigma_{th}\phi_{th}\varepsilon_{th}F_{th}(\lambda,t)}{N_E\sigma_E\phi_E\varepsilon_E F_E(\lambda,t)} \qquad (6)$$

where

ε = efficiency of counting system.

If the same samples and counting system are used for both thermal and E activations, then $N_{th} = N_E$ and $\varepsilon_{th} = \varepsilon_E$.

$$\therefore \quad R = \frac{\sigma_{th}\phi_{th}F_{th}(\lambda,t)}{\sigma_E\phi_E F_E(\lambda,t)} \tag{7}$$

One can write down a similar equation for a standard and take the ratio of R to R_s, where the subscript refers to the standard.

$$\frac{R}{R_s} = \frac{\{\sigma_{th}\phi_{th}F_{th}(\lambda,t)\}}{\{\sigma_E\phi_E F_E(\lambda,t)\}} \quad \frac{\{\sigma_{sE}\phi_{sE}F_{sE}(\lambda,t)\}}{\{\sigma_{sth}\phi_{sth}F_{sth}(\lambda,t)\}} \tag{8}$$

By activating both the standard and the sample in the same thermal flux we may write the above equation, solving for σ_E, as

$$\sigma_E = \frac{R_s}{R} \frac{\phi_{sE}}{\phi_E} \{\frac{\sigma_{th}\sigma_{sE}}{\sigma_{sth}}\} \{\frac{F_{th}(\lambda,t)}{F_{sth}(\lambda,t)}\} \{\frac{F_{sE}(\lambda,t)}{F_E(\lambda,t)}\} \tag{9}$$

Hence, one can determine the absolute cross section by activating a sample and a standard in a thermal flux and in a monoenergetic non-thermal flux, then counting to determine the above ratios. The following thermal neutron cross sections were used to perform this calculation: σ(natural Ag) = 63.6 $\pm$ 0.6 barns, $\sigma(^{107}Ag)$ = 35 $\pm$ 5 barns, $\sigma(^{109}Ag)$ = 89 $\pm$ 4 barns, $\sigma(^{115}In)$ = 157 $\pm$ 4 barns, and $\sigma(^{127}I)$ = 6.2 $\pm$ 0.2 barns[23]. The half lives of the resulting radioisotopes which were used were: $T_{1/2}(^{108}Ag)$ = 2.4 minutes, $T_{1/2}(^{110}Ag)$ = 24 seconds, $T_{1/2}(^{116m}In)$ = 54 minutes, $T_{1/2}(^{128}I)$ = 25 minutes.

For a thermal neutron source, the thermal column of the V.P.I. UTR 100 reactor was used. Each sample was placed in the central

stringer a distance of 102 cm from the lead gamma curtain and activated for one minute at 10 watts. This position yielded an absolute flux of about 10^6 neutrons/cm^2/sec at this power level. At this position the neutron beam is essentially all thermal since the cadmium ratio at a distance of 76 cm is 540 to 1, as shown by Stam[24].

Each sample was activated at 24 keV in the exact geometrical configuration which was used to determine the relative cross sections. By performing the activation of each sample at 24 keV within a short time interval and in identical geometries, we were confident of having a little change in the neutron yield and detector response, enabling us to determine the ratio ϕ_{sE}/ϕ_E accurately. Equation (8) was then used to calculate the absolute cross section at 24 keV. The cross section versus energy curves were then normalized to this value. The entire normalization experiment, including reactor and Van de Graaff irradiations, was performed in a single evening so that activation and counting could be done with a minimum error due to activation geometry and any possible variations in the counting equipment. The results along with values determined by other investigators are given in the next chapter.

B. Average Resonance Parameters

To the nuclear theorists resonance parameters are the most important information to be obtained from this work. These parameters, which will be defined below, tell much about the target nucleus and have meaning in relation to statistical nuclear models such as the optical model.

Before proceeding further it is beneficial to define the more commonly used terms which are to be used.

1) $\sigma_{n\gamma}$ = neutron capture cross section

2) E = incident neutron energy

3) E_o = energy of a particular resonance

4) $\lambda\!\!\!^{-}$ = $1/k$ = de Broglie wavelength of the incident neutron

5) R = radius of the target nucleus = $1.4\ A^{1/3}$ fermis

6) $\bar{I}$ = spin of the target nucleus

7) $\bar{\ell}$ = angular momentum of the incident neutron

8) $\bar{J}$ = $\bar{I} + \bar{\ell} + \overline{1/2}$ = spin of the compound nucleus

9) g_J = statistical weight factor = $\dfrac{2J + 1}{2(2I + 1)}$

10) v_ℓ = penetration factor of the nucleus for neutrons of angular momentum ℓ

11) $\Gamma_n^{(\ell)}$ = reduced width at 1 eV of a resonance with angular momentum ℓ

12) Γ_n = $\Gamma_n^{(\ell)}(\sqrt{E_o}\ v_\ell)$ = neutron width of resonance at energy E_o with angular momentum ℓ

13) Γ_γ = gamma width of the resonance

14) Γ = total width of the resonance at energy E_o

15) s = local level spacing in the neighborhood of a given resonance

16) D_{obs} = (neutron energy interval)/(number of resonances of a given angular momentum in that interval)

17) D_o = $D_{obs} \times 2(2I + 1)(2\ell + 1)$

18) D_J = $D_o/(2J + 1)$

19) $\langle \Gamma_{nJ}^{(\ell)} \rangle / \langle D_J \rangle$ = $(\langle \Gamma_n^{(\ell)} \rangle / \langle D \rangle)_J$ = neutron strength function for an orbital angular momentum ℓ and spin J

20) $\left(\left\langle \Gamma_\gamma \right\rangle / \left\langle D_n \right\rangle\right)_J$ = γ-ray strength function

21) $\left\langle\left\langle \Gamma_{nJ}^{(\ell)} \right\rangle / \left\langle D_J \right\rangle\right\rangle = (2\ell+1)^{-1} \sum_s g_J \left\langle \Gamma_{nJ}^{(\ell)} \right\rangle / \left\langle D_J \right\rangle =$

$\left\langle \Gamma_n^{(\ell)} \right\rangle / \left\langle D \right\rangle$

22) $\left\langle\left\langle \Gamma_{\gamma J} \right\rangle / \left\langle D_n \right\rangle\right\rangle_\ell = \left(\sum_J gJ(2J+1)\right)^{-1} \sum_J g_J \left\langle \Gamma_\gamma \right\rangle / \left\langle D_J \right\rangle =$

$\left\langle \Gamma_\gamma \right\rangle / \left\langle D_o \right\rangle_\ell$

NOTE: In the above definitions and the work that follows, average values are denoted by braces $\langle\ \rangle$. Also, vector quantities are designated by placing a bar above the quantity (See definition 8 above). The notation used herein is from Bilpuch et al[12].

The subscripts in the above definitions indicate that the particular quantity refers to neutrons of a particular angular momentum, ℓ, and resonances of the compound nucleus with spins, J, which can be formed with these neutrons. Subscripts outside parentheses are understood to refer to each enclosed term.

According to the compound nucleus concept of nuclear reactions we may denote the probability of the reaction X(n,γ)X' as

$$\sigma_{n\gamma} = \sigma_c(n) \text{ X (relative prob. of } \gamma\text{-emission)} \qquad (1)$$

where $\sigma_c(n)$ is the cross section for the formation of the compound nucleus. The relative probability of γ-emission is simply Γ_γ/Γ, where Γ_γ is the partial level width for γ and Γ is the total level width. For heavy nuclei (80 < A < 250) and intermediate energy neutrons (1 keV < E < 500 keV) the only reactions which are discernible are (n,γ) capture and elastic scattering[25]. The work done

in this project falls in both categories; therefore, $\Gamma = \Gamma_\gamma + \Gamma_n$.

The Breit-Wigner single level formula[26] gives the theoretical cross section in the case of resonance phenomena. This equation in its simplest form gives the value of the cross section in the neighborhood of a single resonance level formed by neutron capture as

$$\sigma_{n\gamma} = g_J \pi \lambda\!\!\!^{-2} \Gamma_n \Gamma_\gamma / \{(E - E_o)^2 + (\Gamma/2)^2\} \qquad (2)$$

Equation 2 may be thought of as composed of three terms. The first is a measure of the probability of compound nucleus formation and is proportional to $\lambda\!\!\!^{-2}$. The second, $[(E - E_o)^2 + (\Gamma/2)^2]^{-1}$, is the resonance factor and results in maximum values for $\sigma_{n\gamma}$ when $E \sim E_o$. The partial widths Γ_n and Γ_γ give the probabilities for definite types of disintegration of the compound nucleus.

The average cross section for a single resonance of local level spacing, s_J, is given by

$$\langle \sigma_{n\gamma} \rangle = \frac{1}{s_J} \int_{E_o - s_J/2}^{E_o + s_J/2} \sigma_{n\gamma} dE \qquad (3)$$

where $\sigma_{n\gamma}$ is given by Eq. (2). Over this energy region, which contains a single resonance, Γ_γ is a constant and Γ and quantities dependent upon E alone are slowly varying functions of energy and may be assumed constant.

$$\therefore \langle \sigma_{n\gamma} \rangle = \frac{g_J \pi \lambda\!\!\!^{-2} \Gamma_n \Gamma_\gamma}{s_J} \int_{E_o - s_J/2}^{E_o + s_J/2} \frac{dE}{(E - E_o)^2 + (\Gamma/2)^2} \qquad (4)$$

Essentially the entire contribution to the integral is a result of the energy region in the immediate vicinity of the resonance. No significant error is introduced by extending the limits of integration to $\pm \infty$.

$$\therefore \left\langle \sigma_{n\gamma} \right\rangle = \frac{g_J \pi \lambda\!\!\!^{-2} \Gamma_\gamma \Gamma_n}{s_J} \int_{-\infty}^{+\infty} \frac{dE}{(E - E_o)^2 + (\Gamma/2)^2} \qquad (5)$$

and

$$\int_{-\infty}^{+\infty} \frac{dE}{(E - E_o)^2 + (\Gamma/2)^2} = \int_{-\infty}^{\infty} \frac{dx}{a + bx + cx^2}$$

where

$$x = E$$

$$a = E_o^2 + \Gamma^2/4$$

$$b = -2E_o$$

$$c = 1.$$

$$\int_{-\infty}^{+\infty} \frac{dx}{a + bx + cx^2} = \frac{2}{\sqrt{q}} \tan^{-1} \frac{2cx + b}{\sqrt{q}} \Bigg|_{x = -\infty}^{x = \infty}$$

where

$$q = 4ac - b^2 = \Gamma^2 = (\Gamma_n + \Gamma_\gamma)^2 .$$

$$\therefore \left\langle \sigma_{n\gamma} \right\rangle = \frac{g_J 2\pi^2 \lambda\!\!\!^{-2} \Gamma_n}{\Gamma_n + \Gamma_\gamma} \frac{\Gamma_\gamma}{s_J} \qquad (6)$$

We are interested in the average cross section over a region which contains many resonances and which depends on the average value

of the parameters of Eq. (6). Rae, et al[27] have shown that Γ_γ is expected to vary little from level to level, but $\langle \sigma_{n\gamma} \rangle$ does depend upon the distribution chosen for the reduced neutron widths. In general, the average cross section over a region containing many resonances may be written

$$\langle \sigma_{n\gamma} \rangle_{\ell J} = 2\pi^2 \lambda^2 g_J \left[\frac{\langle \Gamma_\gamma \rangle}{\langle D_J \rangle}\right] \left\{\frac{\langle \Gamma_n \rangle}{\langle \Gamma_n \rangle + \langle \Gamma_\gamma \rangle}\right\} F\left(\frac{\langle \Gamma_\gamma \rangle}{\langle \Gamma_n \rangle}\right)_{\ell J} \qquad (7)$$

where $F\left(\frac{\langle \Gamma_\gamma \rangle}{\langle \Gamma_n \rangle}\right)_{\ell J}$ is a correction factor dependent upon the distribution function chosen for $\Gamma_n^{(\ell)} / \langle \Gamma_n^{(\ell)} \rangle$. A Porter-Thomas distribution[28] has been assumed in this work and can be written

$$F(b) = (1 + 2b) \left\{1 - \frac{2\sqrt{b}\,[1 - H\sqrt{b}]}{H'\sqrt{b}}\right\} \qquad (8)$$

where

$$b = \frac{1}{2\sqrt{E}\, v_\ell} \langle \Gamma_\gamma \rangle / \langle \Gamma_n^{(\ell)} \rangle \quad ;$$

$$H(\sqrt{b}) = \frac{2}{\sqrt{\pi}} \int_0^{\sqrt{b}} e^{-t^2}\, dt \quad \text{and} \quad H'(\sqrt{b}) = \frac{2}{\sqrt{\pi}}\, e^{-b}$$

are the tabulated error function and its derivative. Equation (8) is plotted in Fig. (10).

The variable, v_ℓ, above is the penetration factor of the nucleus for a neutron of angular momentum ℓ, and has the values

$$\begin{aligned} v_0 &= 1 \\ v_1 &= k^2R^2/(1 + k^2R^2) \\ v_2 &= k^4R^4/(9 + 3k^2R^2 + k^4R^4) \end{aligned} \qquad (9)$$

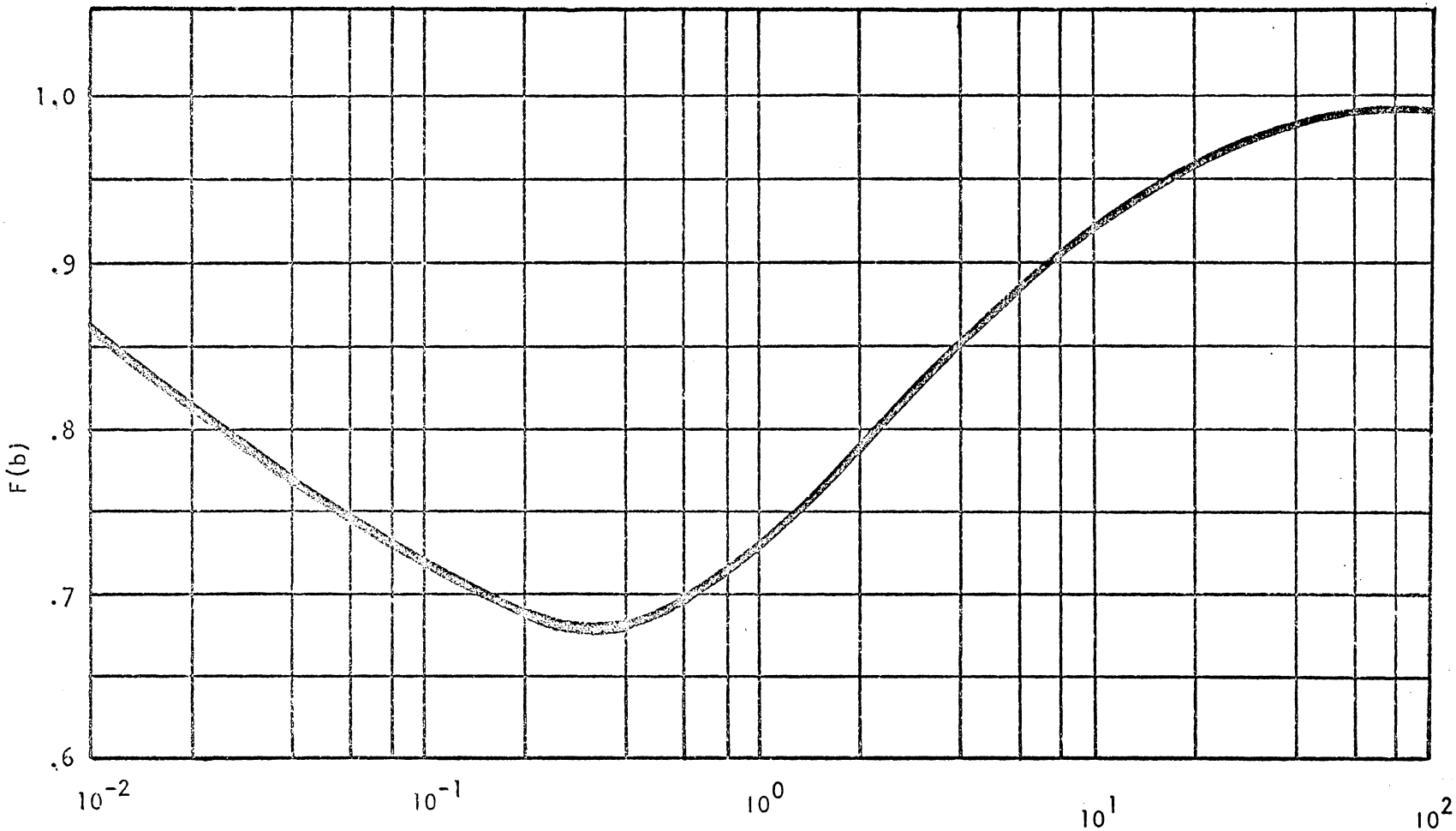
1.0
.9
.8
.7
.6
F(b)
10^{-2}
10^{-1}
10^{0}
10^{1}
10^{2}
$b = 1/2 \langle \Gamma_\gamma \rangle / \langle \Gamma_n \rangle$

FIGURE 10

By having an upper limit of 155 keV for the neutron energy in this experiment, it is assumed that only s- and p-wave neutrons are present; therefore, we have values of 0 and 1 for ℓ. This assumption perhaps is not a rigorously valid one, but analysis for d-wave contributions is severely limited by the accuracy of the data available.

Some further assumptions are made before Eq. (7) can be used to analyze the cross section data. It has been shown empirically[29] that $\Gamma_\gamma/D_J^{(\ell)}$ is proportional to $(2J + 1)^{-5/4}$. If it is assumed that $D_o = (2J + 1)D_J$ then Γ_γ/D_o is at most proportional to $(2J + 1)^{-1/4}$. Because of this weak J dependence we call $\langle \Gamma_\gamma \rangle / \langle D_o \rangle$ the γ-ray strength function and is taken to be independent of J and E_n for a particular neutron angular momentum. Another widely used assumption is that the neutron strength function, $\langle \Gamma_{nJ}^{(\ell)} \rangle / \langle D_J^{(\ell)} \rangle$, is independent of J, i.e. $\Gamma_n^{(\ell)} = (2J + 1)\Gamma_{nJ}^{(\ell)}$. This allows us to redefine the neutron strength function as $\langle \Gamma_n^{(\ell)} \rangle / \langle D \rangle = (2\ell + 1)^{-1} \sum_J g_J \langle \Gamma_{nJ}^{(\ell)} \rangle / \langle D_J \rangle$.

With the above assumptions, along with $g_J = (2J + 1)/[2(2I + 1)]$, Eq. (7) becomes

$$\langle \sigma_{n\gamma} \rangle_{\ell J} = 2\pi^2\lambda^2 \left\{\frac{(2J + 1)^2}{2(2I + 1)}\right\} \left(\frac{\langle \Gamma_\gamma \rangle}{\langle D_o \rangle}\right)_\ell \left\{\frac{1}{1 + \left(\frac{\langle \Gamma_\gamma \rangle}{\langle \Gamma_n \rangle}\right)_{\ell J}}\right\} F(b) \quad (10)$$

By considering only s- and p-wave contributions there are four parameters to be extracted from Eq. (10). These are $(\langle \Gamma_\gamma \rangle / \langle D_o \rangle)_{\ell=0}$, $(\langle \Gamma_\gamma \rangle / \langle D_o \rangle)_{\ell=1}$, $\langle \Gamma_\gamma \rangle / \langle \Gamma_n^o \rangle$, and $\langle \Gamma_\gamma \rangle / \langle \Gamma_n^1 \rangle$. The last

two of these parameters and the ratio $(\langle \Gamma_\gamma \rangle / \langle D_o \rangle)_{\ell=1} / (\langle \Gamma_\gamma \rangle / \langle D_o \rangle)_{\ell=0}$ are obtained from comparison to the shapes of the cross section versus energy curves while $(\langle \Gamma_\gamma \rangle / \langle D_o \rangle)_{\ell=0}$ and $(\langle \Gamma_\gamma \rangle / \langle D_o \rangle)_{\ell=1}$ are dependent upon the magnitude of the cross sections. There are two methods of analysis: the so-called "two parameter fit" whereby the ratio $(\langle \Gamma_\gamma \rangle / \langle D_o \rangle)_{\ell=1} / (\langle \Gamma_\gamma \rangle / \langle D_o \rangle)_{\ell=0}$ is taken to be unity, and the "three parameter fit" where this ratio can have any value. It has been assumed in this analysis that $(\langle \Gamma_\gamma \rangle / \langle D_o \rangle)_{\ell=0} = (\langle \Gamma_\gamma \rangle / \langle D_o \rangle)_{\ell=1}$. This assumption is in agreement with Lane and Lynn[36], Gibbons et al[9], and Furr[30]. Although this assumption has been shown not to hold strictly[12], the relatively poor accuracy of our cross section curves makes any attempt to extract a three parameter fit futile. The uncertainties in the resulting resonance parameters would be so large as to make the values meaningless.

Average resonance parameters were determined by calculating $\langle \sigma_{n\gamma} \rangle_{\ell J}$ using Eq. (10) for each compound nucleus spin and each neutron angular momentum, with the requirement

$$\langle \sigma_{n\gamma} \rangle = \sum_{\ell} \sum_{J} (\sigma_{n\gamma})_{\ell J} \qquad (11)$$

This was accomplished by assuming that $(\langle \Gamma_\gamma \rangle / \langle D_o \rangle)_{\ell=0} = (\langle \Gamma_\gamma \rangle / \langle D_o \rangle)_{\ell=1} = 1$ and generating the families of curves obtained when different values were substituted for $(\langle \Gamma_\gamma \rangle / \langle \Gamma_n \rangle)_{\ell J}$ in Eq. (10). Figures (11) and (12) illustrate these curves for s- and p-waves, respectively, for ^{107}Ag with the assumption of a Porter-Thomas

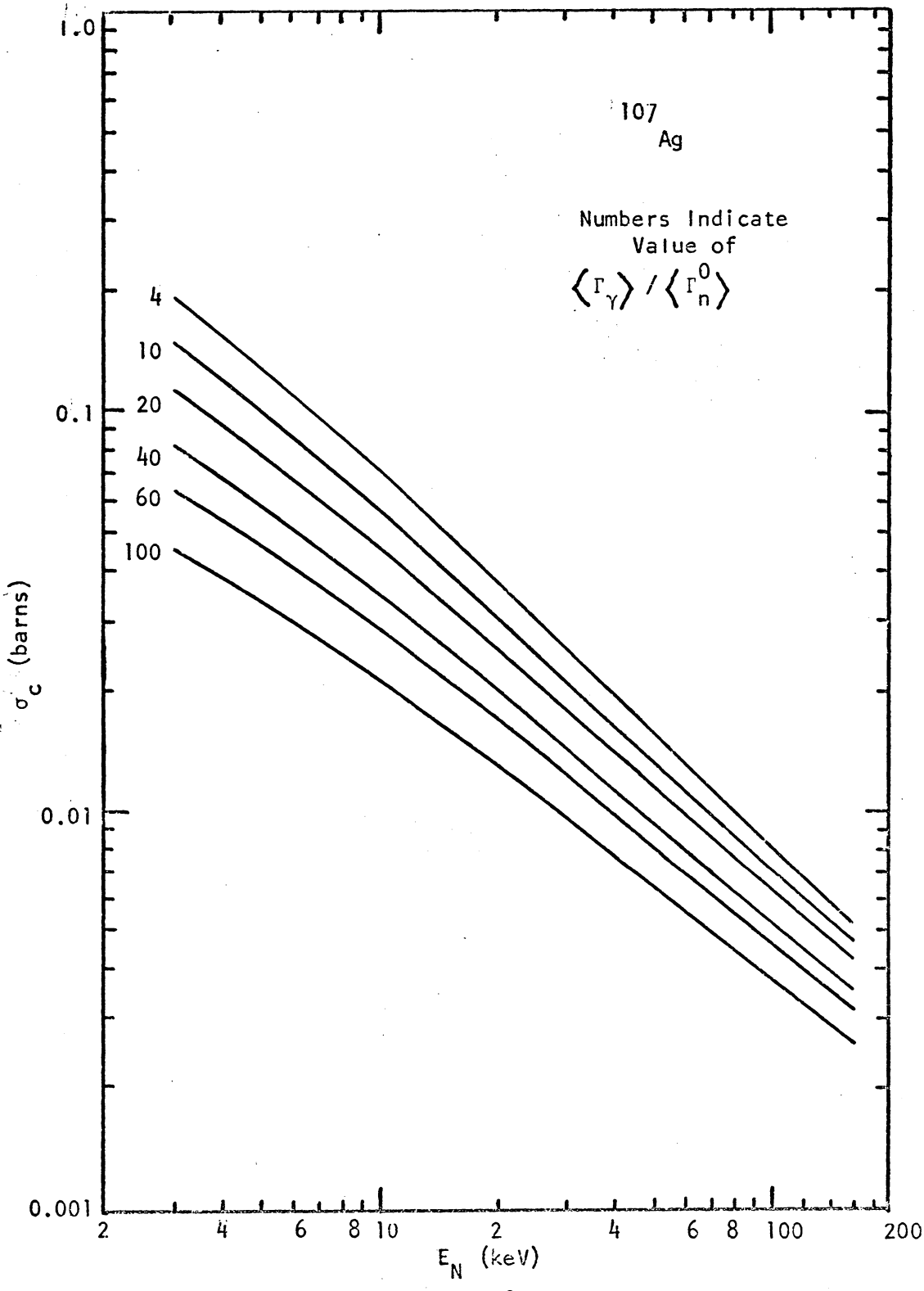

s-wave Components
FIGURE 11

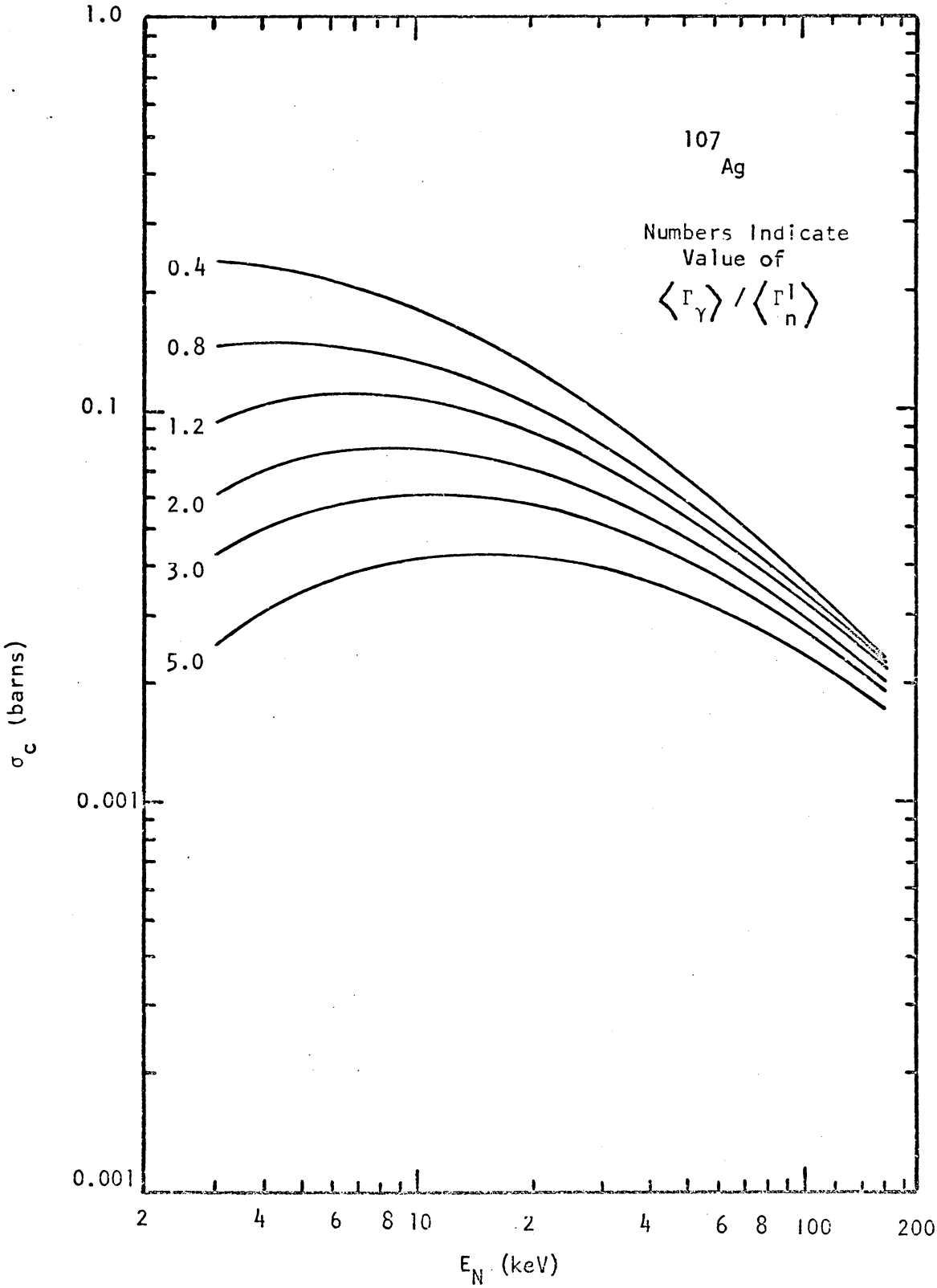

p-wave Components
FIGURE 12

distribution for ($\Gamma_n^{(\ell)} / \langle \Gamma_n^{(\ell)} \rangle$) and indicated values for the ratio $\langle \Gamma_\gamma \rangle / \langle \Gamma_n^{(\ell)} \rangle$. The analysis reduces to choosing a particular curve from each of the s- and p-wave families which, when added together, yields the same shape as the cross section curves previously determined. Figure (13) illustrates the components which were found to be the best fit for ^{107}Ag. By then normalizing the s- and p-wave combination to the absolute value of the cross section at 24 keV calculated earlier, one has found the value of $(\langle \Gamma_\gamma \rangle / \langle D_o \rangle)_{\ell=0} = (\langle \Gamma_\gamma \rangle / \langle D_o \rangle)_{\ell=1}$ as the multiplicative constant necessary for normalization.

Results of this analysis are given in Chapter (VII) and can be compared to values derived by other workers which are also given.

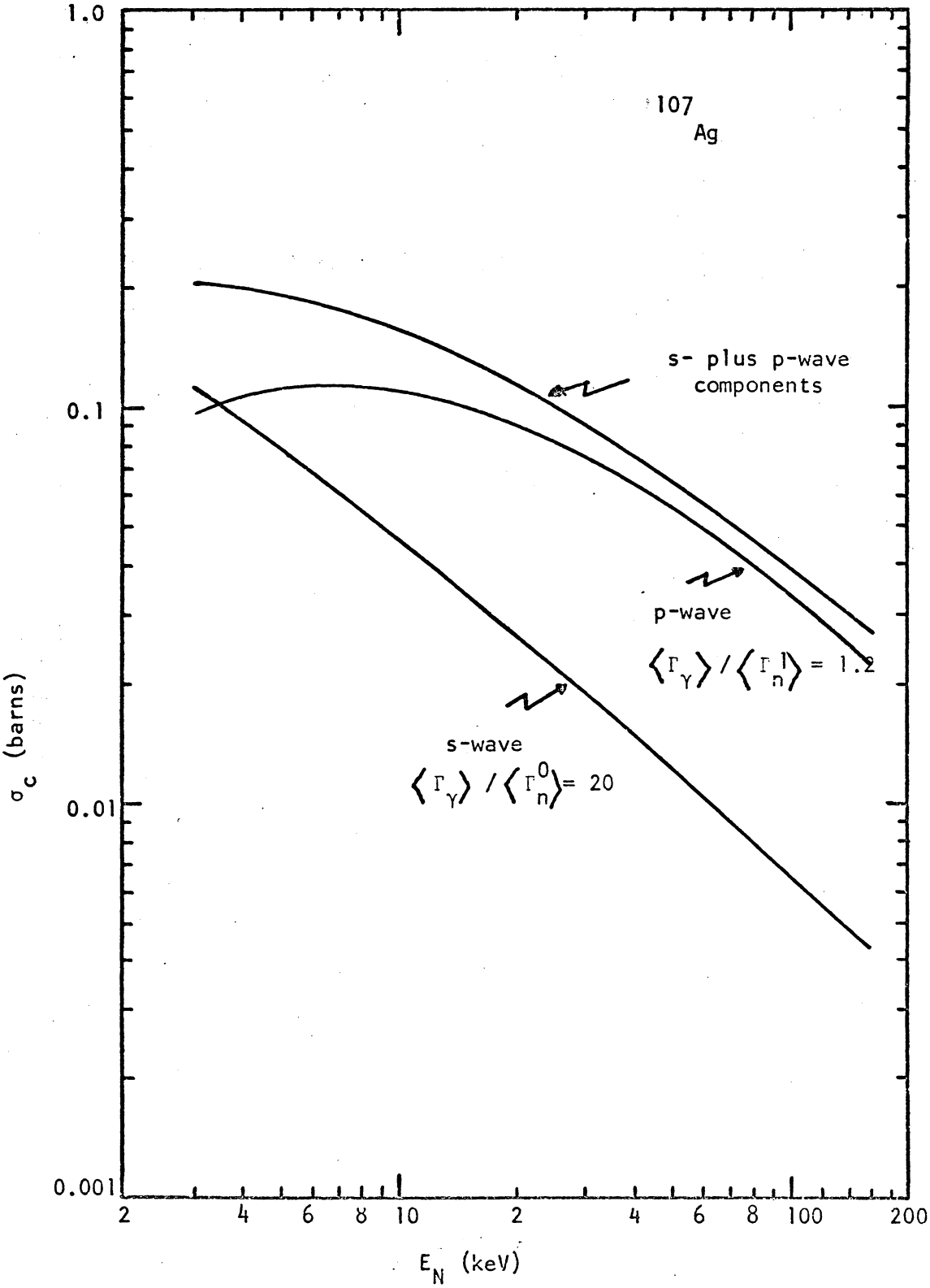

Sum of s- and p-wave Components

FIGURE 13

RESULTS

A. Capture Cross Sections.

The cross sections determined in this experiment are plotted in Figures 14 through 18 with representative error bars. The horizontal error bars (energy spread) were determined from an examination of Figure 3. These error bars consist of a spread in E_n resulting from ^{7}Li target thickness and the angle intercepted by the sample. These values can be compared to the results of other workers given in Figures 19 through 22. The solid lines drawn in Figures 19-22 are the best estimate of the cross sections as a function of energy. It is noted that the cross section curves are reproduced directly from reference 23. On the pages immediately following each figure are found the keys to the various symbols used and the experimenters who determined the values. The capture cross sections determined herein are in general good agreement with values of other workers, with the greatest deviations appearing in the ^{107}Ag and ^{109}Ag isotopes. Even in these two cases, the error bars of the data in this experiment overlap those of other workers.

Even though our values are in good agreement with others as indicated above, as far as the magnitude of the cross sections is concerned, there are variations compared to the shapes of the cross section curves from other sources. These variations are not consistent from isotope to isotope and cannot be attributed to a systematic error in our analysis.

Comments on the individual nuclei follow, including comparison

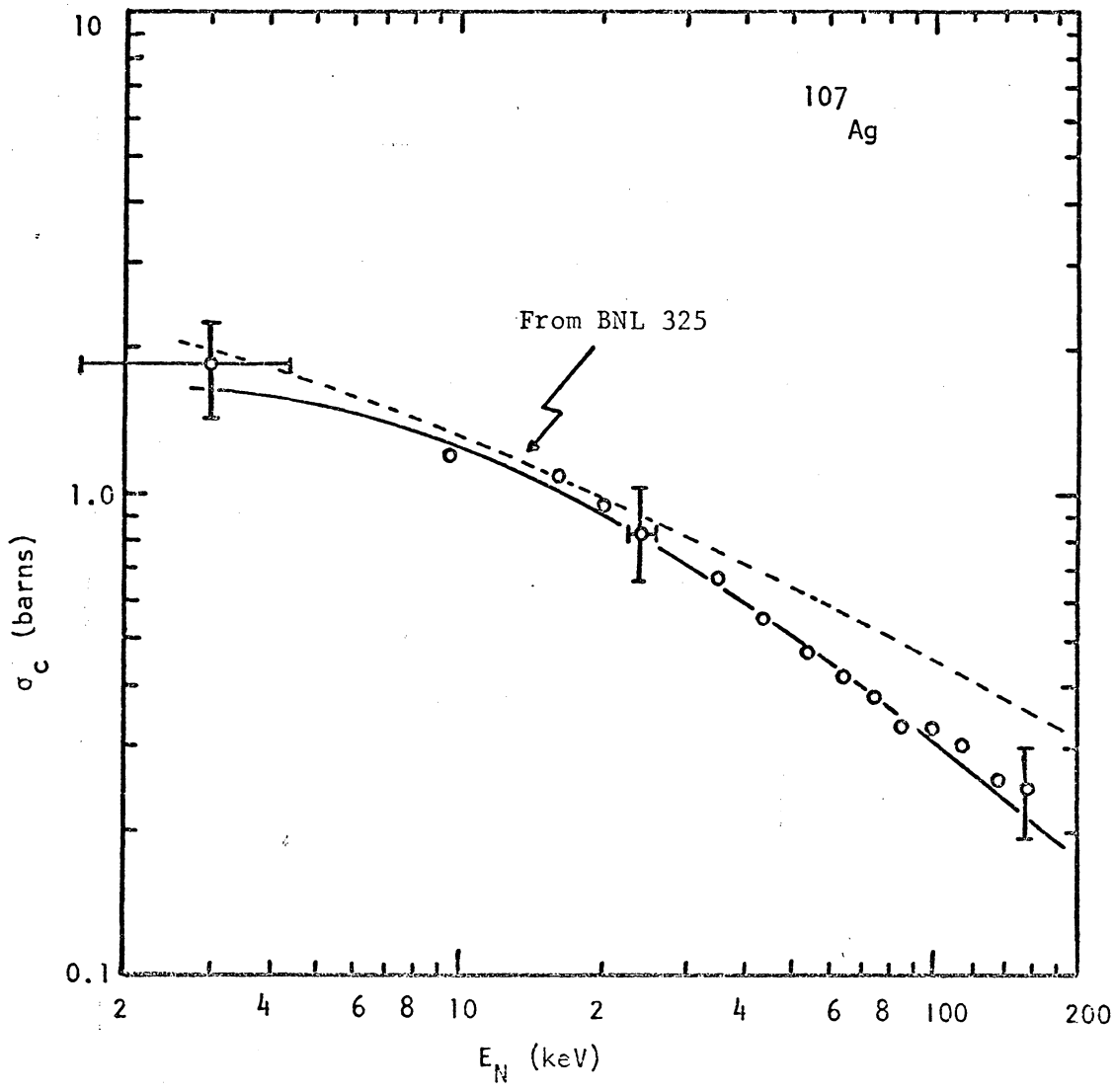
10
1.0
0.1
σ_c (barns)
107
Ag
From BNL 325
2
4
6
8
10
2
4
6
8
100
200
E_N (keV)

FIGURE 14

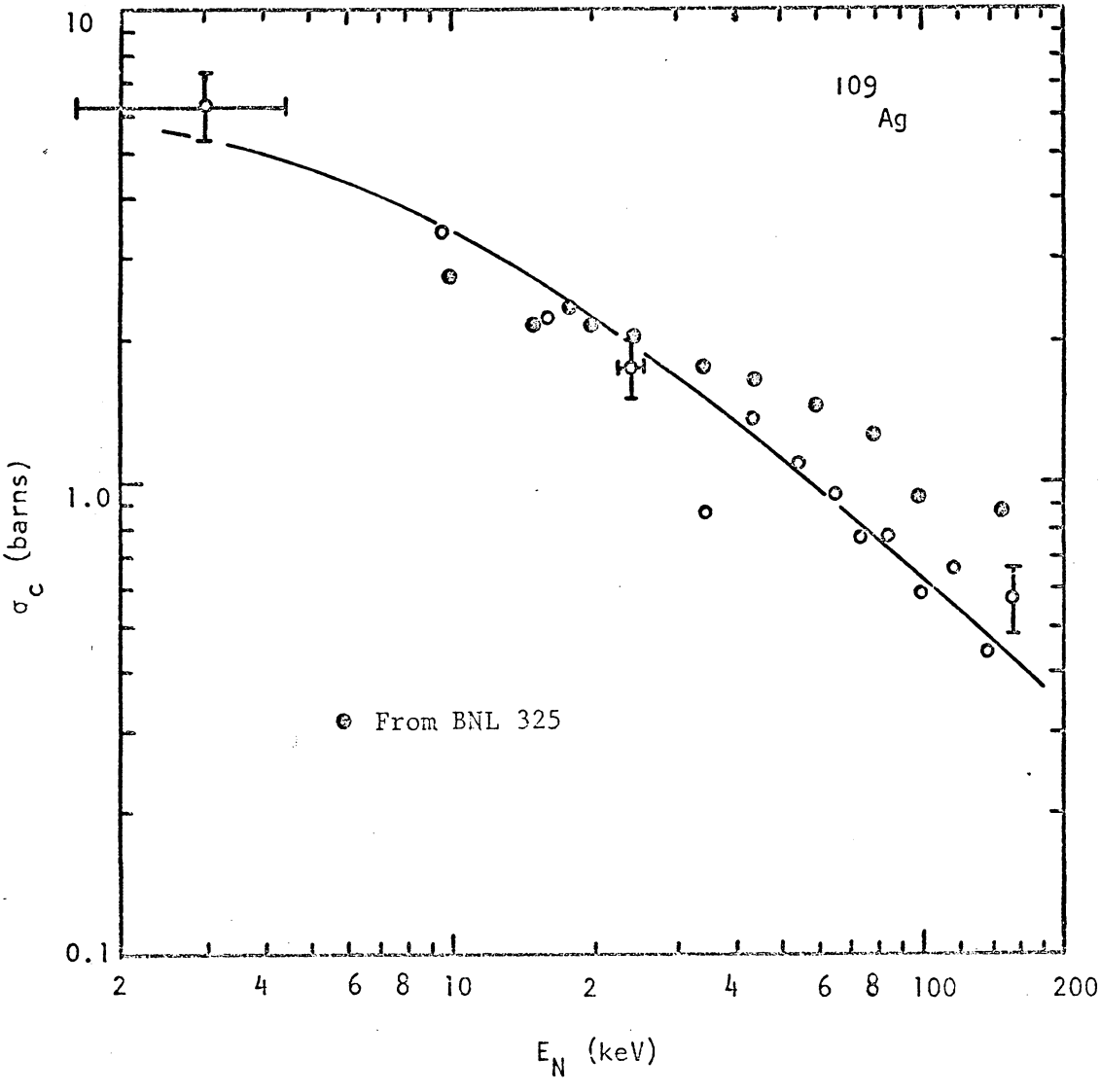
10
1.0
0.1
σ_c (barns)
109
Ag
From BNL 325
2
4
6
8
10
2
4
6
8
100
200
E_N (keV)

FIGURE 15

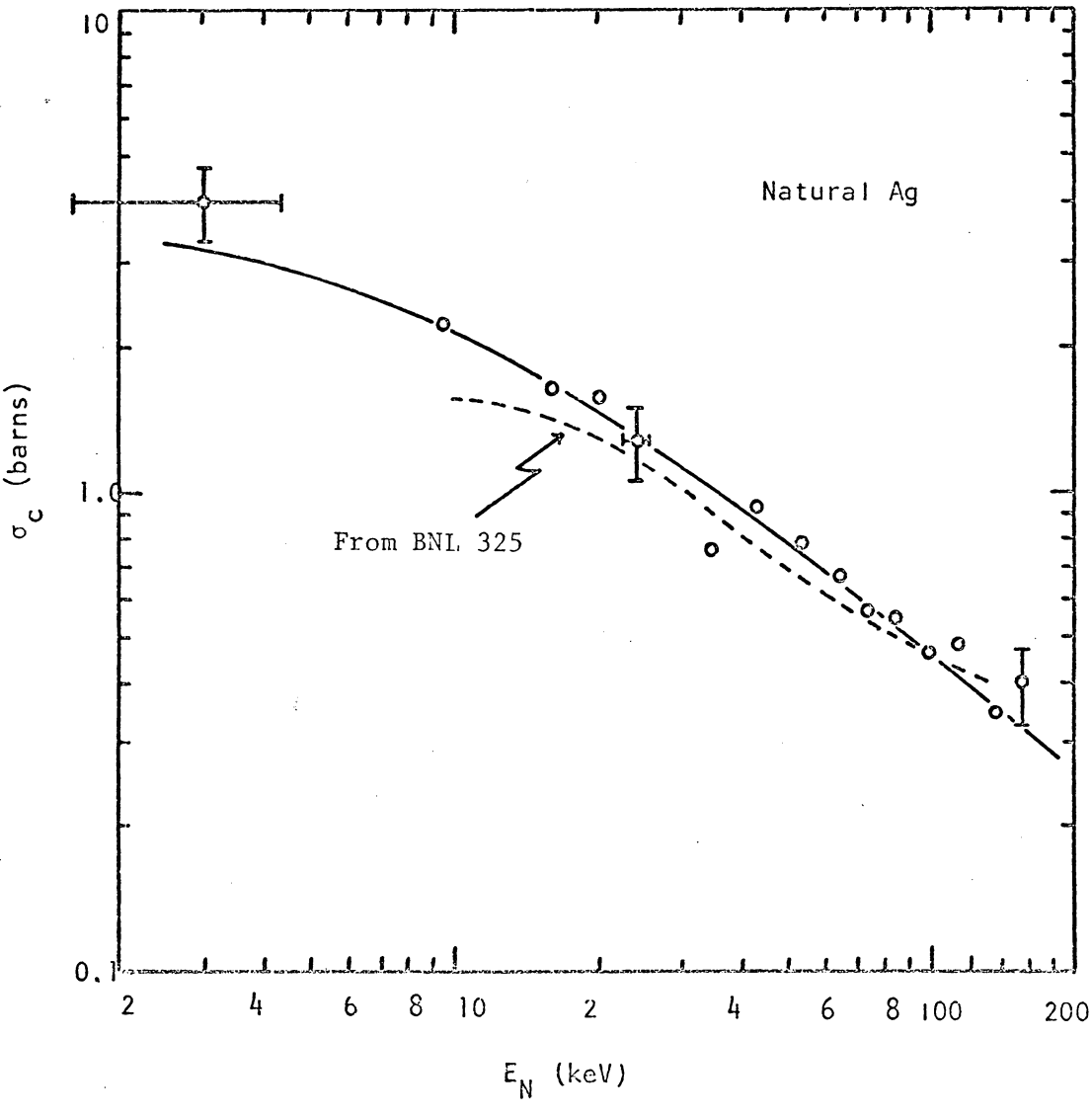
10
1.0
0.1
σ_c (barns)
Natural Ag
From BNL 325
2
4
6
8
10
2
4
6
8
100
200
E_N (keV)

FIGURE 16

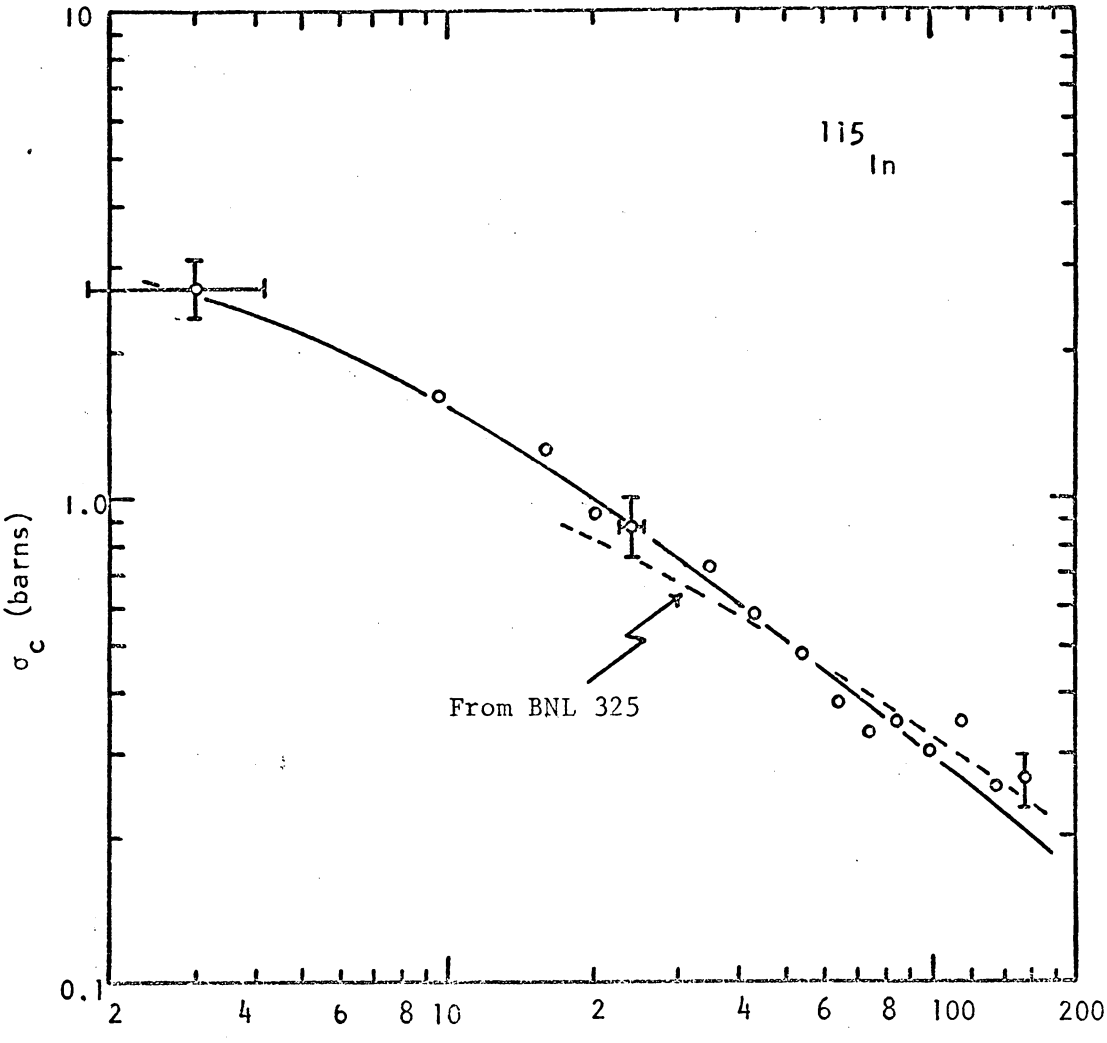
10
1.0
0.1
σ_c (barns)
115 In
From BNL 325
2
4
6
8
10
2
4
6
8
100
200
E_N (keV)

FIGURE 17

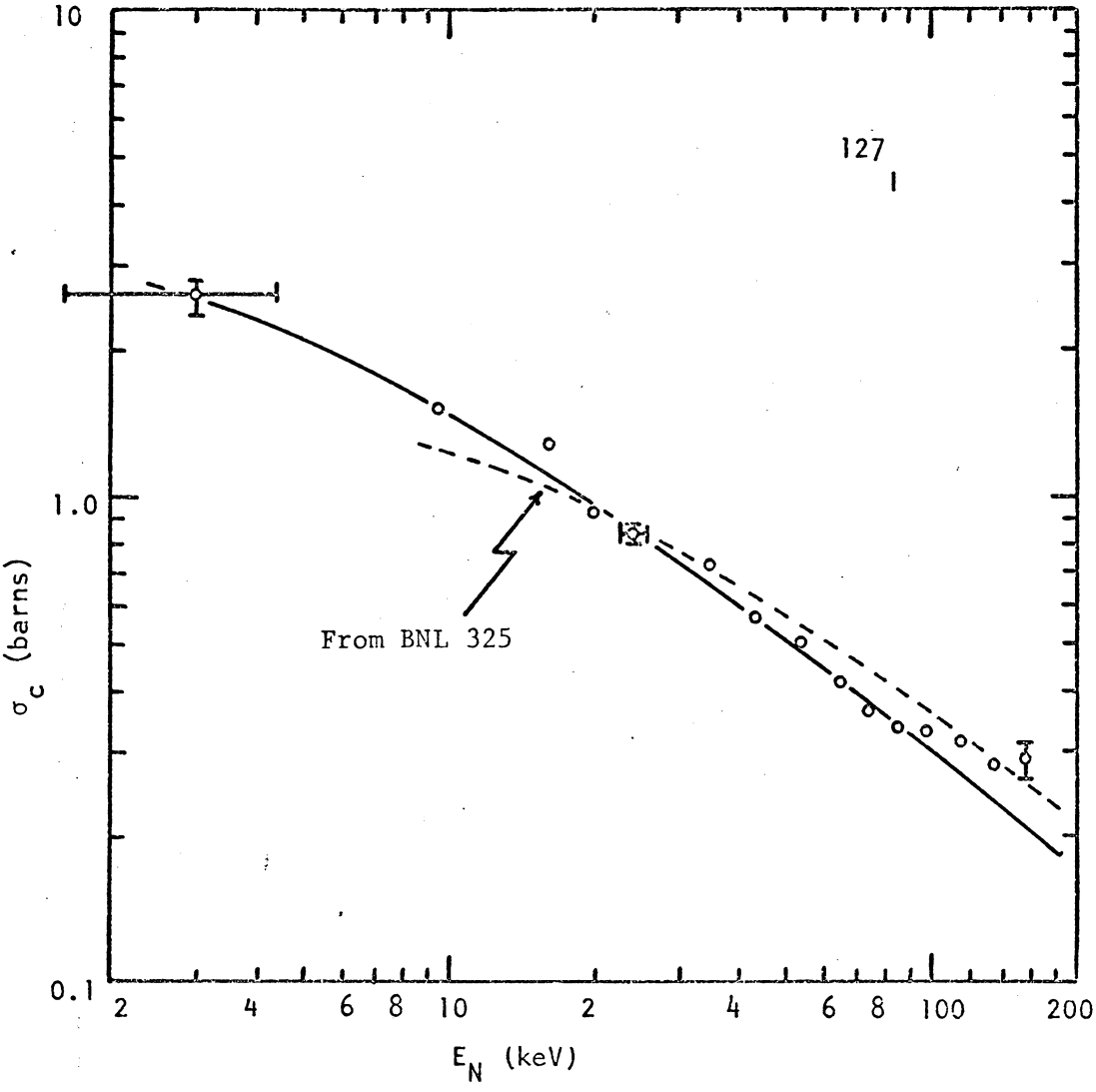
10
1.0
0.1
σ_c (barns)
127
I
From BNL 325
2
4
6
8
10
2
4
6
8
100
200
E_N (keV)

FIGURE 18

with other workers of our value of the cross section at 24 keV, relative to $^{127}I(n,\gamma)$ σ = 0.832 $\pm$ .026 barns at 24 keV. The symbols refer to the same symbols used on the respective graphs.

^{107}Ag, Figures 14 and 19. The values determined in this experiment all lie beneath the curve of published values but the discrepancy is not great except above 30 keV, where the slope of our cross section curve is greater than that of other workers. Values for the cross section at 24 keV are: This work, $\sigma_{n\gamma}$ = 0.830 $\pm$ .180 barns; □ , $\sigma_{n\gamma}$ = 1.75 $\pm$ .20 barns; ▣ , $\sigma_{n\gamma}$ = 1.31 $\pm$ .09 barns; ∇ , $\sigma_{n\gamma}$ = 0.93 $\pm$ .08 barns; ▲ , $\sigma_{n\gamma}$ = 0.84 $\pm$ .10 barns.

^{109}Ag, Figures 15 and 19. Only one set of values is given for comparison. ^{109}Ag, having a 24 second half life, is difficult to examine by transferring of the sample between activation and counting, and the statistics of this isotope are the worst of the nuclides studied in this work. In comparing the cross section curve determined in this experiment with that plotted(x) due to Weston, et al., we see that our curve crosses his at about 20 keV with a considerably greater slope. However, the large error bars on our data illustrate an inability to have much faith in the results. Our value of the cross section at 24 keV is $\sigma_{n\gamma}$ = 1.74 $\pm$ .26 barns. The value interpolated from Weston's data is $\sigma_{n\gamma}$ = 2.15 barns.

Natural Ag, Figures 16 and 20. Our results for natural Ag are in good agreement with the curve of accepted values given in Fig. 20. The major discrepancy is the value at the lowest energy, where our curve lies considerably above the published values. Values at 24 keV

are: This work, $\sigma_{n\gamma} = 1.27 \pm .22$ barns; □ , $\sigma_{n\gamma} = 0.98 \pm .06$ barns; ◇ , $\sigma_{n\gamma} = 1.12 \pm .08$ barns.

^{115}In, Figures 17 and 21. Again, good agreement was found between published values and values determined in this experiment. However, the slope of the two curves shown in Figures 17 and 21 are not the same. Cross sections at 24 keV are: This work, $\sigma_{n\gamma} = 0.88 \pm .12$ barns; ◆ , $\sigma_{n\gamma} = 0.58 \pm .04$ barns; ◇ , $\sigma_{n\gamma} = 0.77 \pm .05$ barns.

^{127}I, Figures 18 and 22. Results of our analysis for ^{127}I are in excellent agreement with values given by other workers. Slight differences, however, can be seen in the shape of the curve. Cross sections at 24 keV are: This work, $\sigma_{n\gamma} = 0.832 \pm .032$ barns; ▩ (value taken as standard), $\sigma_{n\gamma} = 0.832 \pm .026$ barns; + , $\sigma_{n\gamma} = 0.768 \pm .09$ barns; ▨ , $\sigma_{n\gamma} = 0.99 \pm .04$ barns; ◍ , $\sigma_{n\gamma} = 0.820 \pm .06$ barns.

B. Average Resonance Parameters.

The results of our analysis for determining the average resonance parameters are given in Tables I-V, along with values measured by other workers. The quoted errors for the parameters calculated in the present work are a measure of the uniqueness of the fit of the s- and p-wave components to the experimental cross section curve. Some results are in good agreement with other experimenters, while others differ greatly.

S-Wave Neutron Strength Functions, Column 4. The measured s-wave neutron strength function, $S_o = \langle \Gamma_n^0 \rangle / \langle D \rangle$, is highly dependent upon the shape of the cross section curve at low energies

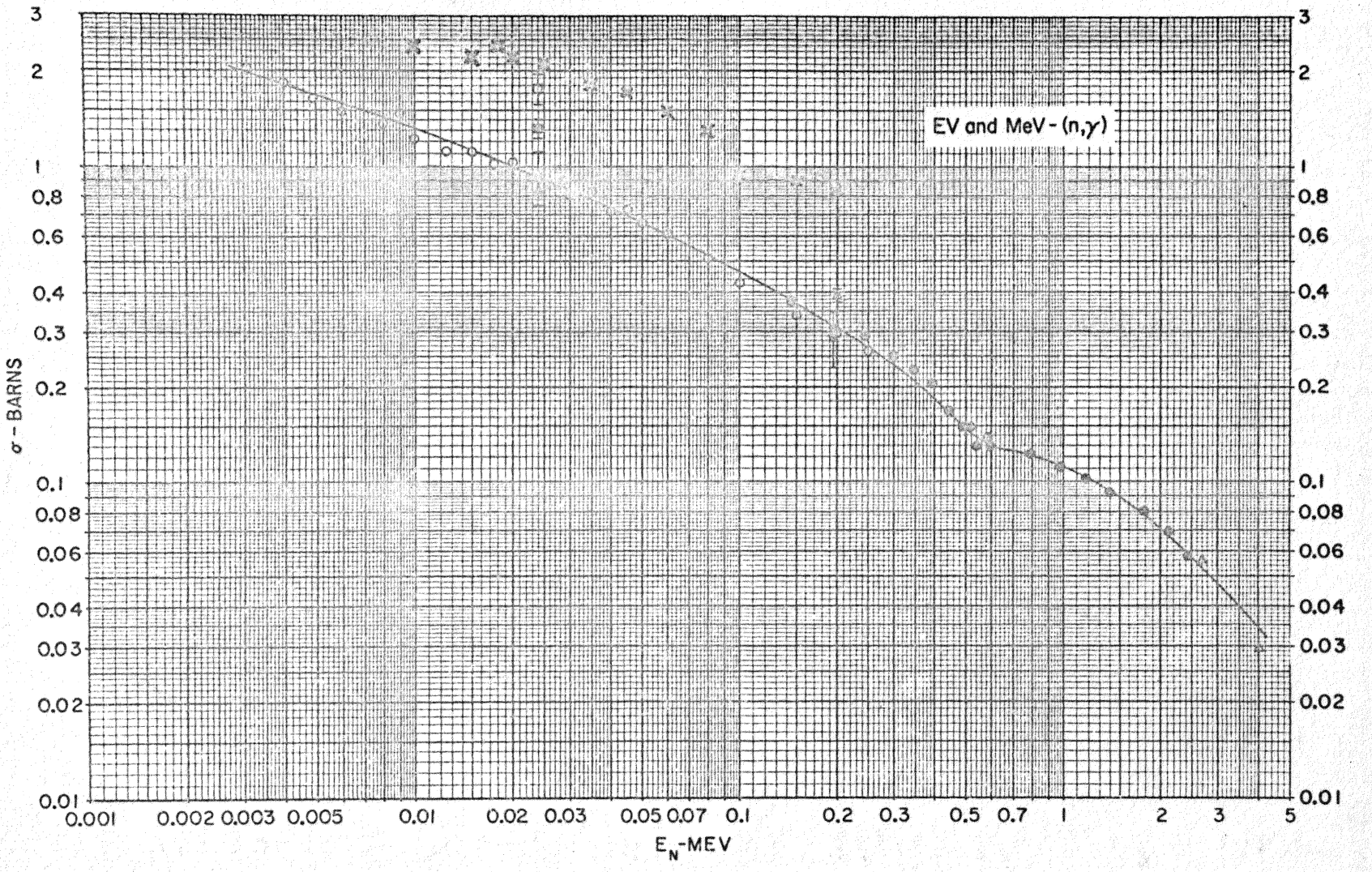

FIGURE 19. ^{109}Ag (crosses) and ^{107}Ag (lower curve).

^{107}Ag

▲ A. K. Chaubey and M. L. Sehgal, Nuclear Phys. 66, 267 (1965). [Aligarh, India]. Counted ^{108}Ag decay betas. Sb–Be source. Relative to I (n,γ) σ = 820 mb.

○ L. W. Weston, K. K. Seth, E. G. Bilpuch, and H. W. Newson, Ann. Phys. 10, 477 (1960). [Duke]. Counted ^{108}Ag decay betas. Normalized to data of Lyon and Macklin 59, below and Macklin, et al. 57, below.

◐ A. E. Johnsrud, M. G. Silbert, and H. H. Barschall, Phys. Rev. 116, 927 (1959). [Wisconsin]. Counted gammas following ^{108}Ag decay. Relative to ^{107}Ag thermal (n,γ) σ = 45 $\pm$ b and to ^{235}U σ_F. Renormalized here to ^{107}Ag thermal (n,γ) σ = 35 b and to the ^{235}U σ_F curve in Vol. III, Reference 23.

▼ W. S. Lyon and R. L. Macklin, Phys. Rev. 114, 1619 (1959). [Oak Ridge]. Counted 610 keV gamma following ^{108}Ag decay. RdTh–D_2O source. Relative to ^{115}In (54 min) (n,γ) σ = 195 $\pm$ 10 mb at 195 keV.

□ J. F. Vervier, Nuclear Phys. 9, 569 (1958/59). [Louvain]. Counted ^{108}Ag decay betas. Sb–Be source. Relative to ^{115}In (54 min) (n,γ) σ = 825 $\pm$ 75 mb and Au (n,γ) σ = 1065 $\pm$ 95 mb at 25 keV.

▩ V. N. Kononov, Yu. Ya. Stavisskii, and V. A. Tolstikov, Atomnaya Energiya 5, 564 (1958). [Transl. in J. Nuclear Energy, 11, 46 (1959/60)]. Counted ^{108}Ag decay betas. Sb–Be source.

Relative to I (n,γ) σ = 820 $\pm$ 60 mb at 25 keV.

Δ A. I. Leipunsky, O. D. Kazachkovsky, G. Y. Artyukhov, A. I. Baryshnikov, T. S. Belanova, V. N. Galkov, Y. Y. Stavissky, E. A. Stumbur, and L. E. Sherman, Second Geneva Conf., Vol. 15, p. 50, paper P/2219 (1958). Measured ^{108}Ag decay. Relative to I (n,γ) σ.

∇ R. L. Macklin, N. H. Lazar, and W. S. Lyon, Phys. Rev. 107, 504 (1957). [Oak Ridge]. Counted 610 keV gamma following ^{108}Ag decay. Sb-Be source. Relative to I (n,γ) σ = 820 $\pm$ 60 mb.

^{109}Ag

X L. W. Weston, K. K. Seth, E. G. Bilpuch, and H. W. Newson, Ann. Phys. Vol. 10, 477 (1960). [Duke]. Counted ^{110}Ag decay betas.

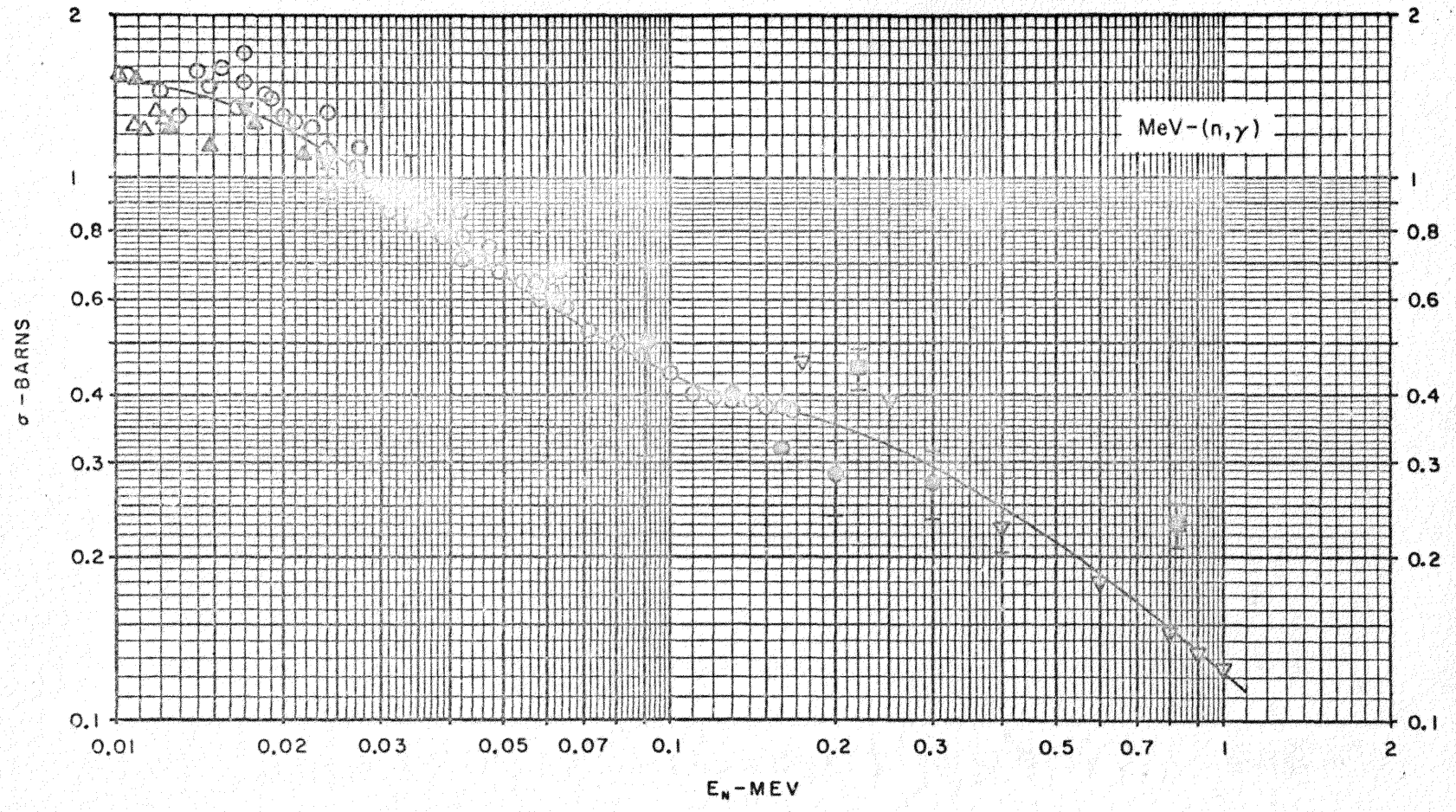

FIGURE 20. Natural Ag.

NATURAL Ag

□ T. S. Belanova, A. A. Van'kov, F. F. Mikhailus, and Yu. Ya. Stavisskii, Atomnaya Energiya 19, 3 (1965). Sphere transmission measurement. Sb-Be source.

Δ M. C. Moxon and E. R. Rae, Nuclear Instr. and Methods 24, 445 (1963), and private communication (1964). [Harwell]. Moxon-Rae detector. Time-of-flight. Normalized to resonance data at low energies.

▲ E. Haddad, S. Friesenhahn, and W. M. Lopez, GA-3874 (1963) and private communication (1964). [General Atomic]. Large liquid scintillator array. Preliminary thin target data.

◍ I. Bergqvist, Arkiv. Fysik 23, 425 (1963). [Research Inst. National Defense, Stockholm]. Counted gammas. NaI scintillator. Normalized to σ = 1185 mb at 24 keV.

O J. H. Gibbons, R. L. Macklin, P. D. Miller, and J. H. Neiler, Phys. Rev. 122, 182 (1961). [Oak Ridge]. Large liquid scintillator tank. Relative to In (n,γ) σ.

▽ B. C. Diven, J. Terrell, and A. Hemmendinger, Phys. Rev. 120, 556 (1960). [Los Alamos]. Large liquid scintillator tank. Relative to ^{235}U capture + fission σ.

▩ T. S. Belanova, Atomnaya Energiya 8, 549 (1960). [Transl. in Soviet J. Atomic Energy 8, 462 (1961)]. Sphere transmission measurement. Sb-Be, Na-D_2O sources. Corrected for multiple scattering.

◊ H. W. Schmitt and C. W. Cook, Nuclear Phys. 20, 202 (1960). [Oak Ridge]. Sphere transmission measurement. Sb-Be source. [Value plotted is the corrected value as presented by H. W. Schmitt at the Neutron Flux Determination Symposium, Oxford, 1963. See EANDC-33 "U".]

▼ A. I. Isakov, Yu. P. Popov, and F. L. Shapiro, Zhur. Eksp. i Teoret. Fiz. 38, 989 (1960). [Lebedev Inst.]. [Transl. in Soviet Phys.-JETP 11, 712 (1960)], Slowing-down-time spectrometer.

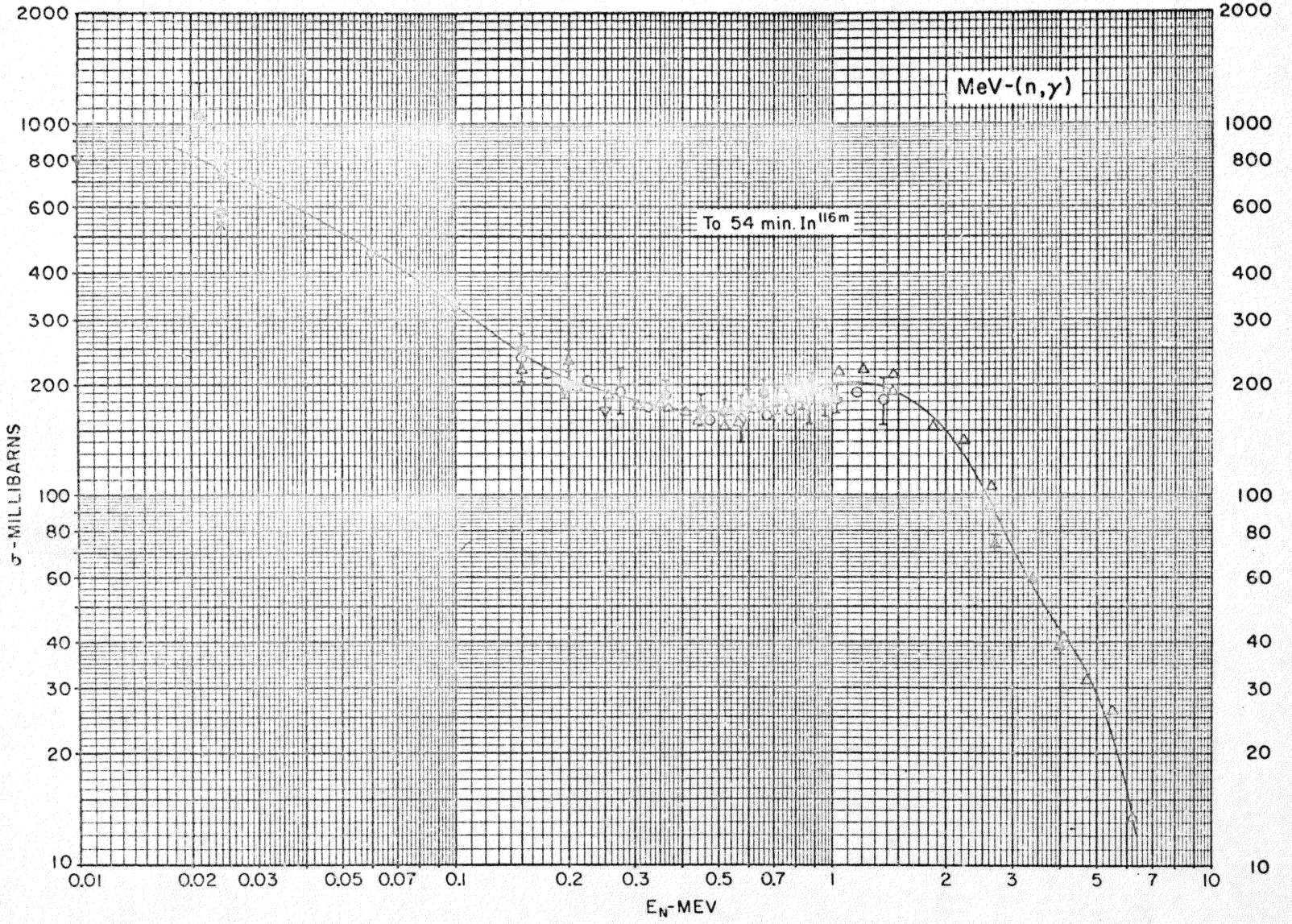

FIGURE 21. ^{115}In

^{115}In

◆ A. K. Chauby and M. L. Sehgal, Nuclear Phys. 66, 267 (1965). [Aligarh, India]. Counted ^{116}In decay betas. Sb-Be source. Relative to I (n,γ) σ = 820 mb.

◇ T. S. Belanova, A. A. Yan'kov, F. F. Mikhailus, and Yu. Ya. Stavisskii, Atomnaya Energiya 19, 3 (1965). Sphere transmission measurement. Sb-Be source.

○ S. A. Cox, Phys. Rev. 133, B378 (1964). [Argonne]. Counted ^{116}In decay betas. Relative to ^{115}In thermal (n,γ) σ = 52 b (to ^{116g}In) and 155 b (to ^{116m}In), and to ^{235}U σ_F. Renormalized here to ^{115}In thermal (n,γ) σ = 42 b (to ^{116g}In), and to ^{235}U σ_F curve in Vol. III, Reference 23.

◉ H. A. Grench and H. O. Menlove, Bull. Am. Phys. Soc. 8, 478 (1963), Bull. Am. Phys. Soc. 9, 21 (1964), and private communication (1966). [Lockheed]. Counted decay gammas. Relative to Au (n,γ) σ. Preliminary data.

▽ L. W. Weston, K. K. Seth, E. G. Bilpuch, and H. W. Newson, Ann. Phys. 10, 477 (1960). [Duke]. Counted ^{116}In decay betas. Normalized to data of Johnsrud, et al. 59, below.

△ A. E. Johnsrud, M. G. Silbert, and H. H. Barschall, Phys. Rev. 116, 927 (1959). [Wisconsin]. Counted gammas following ^{116}In decay. Relative to ^{115}In thermal (n,γ) σ = 155 ± 10 b (to ^{116m}In) and to ^{235}U σ_F. Renormalized here to ^{235}U σ_F curve in Vol. III, Reference 23.

W. S. Lyon and R. L. Macklin, Phys. Rev. 114, 1619 (1959). [Oak Ridge]. Counted 1.28 MeV gamma following ^{116}In decay. RdTh-D_2O source. Relative to ^{115}In (54 min) (n,γ) σ = 195 $\pm$ 10 mb at 195 keV.

R. Booth, W. P. Ball, and M. H. MacGregor, Phys. Rev. 112, 226 (1958). [Livermore]. Counted ^{116}In decay betas and gammas. Sb-Be source. Relative to I (n,γ) σ = 820 $\pm$ 60 mb at 25 keV and 5.5 $\pm$ 0.5 b at thermal, and normalized to ^{115}In thermal (n,γ) σ = 145 b (to ^{116m}In). Renormalized here to ^{116}In thermal (n,γ) σ = 157 b (to ^{116m}In). [Corrections to cross section for change in I (n,γ) σ due to energy re-assignment (25 keV to 20 keV) and for Recommended I thermal (n,γ) σ = 6.2 b cancel each other.]

V. N. Kononov, Yu. Ya. Stavisskii, and V. A. Tolstikov, Atomnaya Energiya 5, 564 (1958). [Transl. in J. Nuclear Energy 11, 46 (1959/60)]. Counted ^{116}In decay betas. Sb-Be source. Relative to I (n,γ) σ = 820 $\pm$ 60 mb at 25 keV.

A. I. Leipunsky, O. D. Kazachkovsky, G. Y. Artyukhov, A. I. Baryshnikov, T. S. Belanova, V. N. Galkov, Y. Y. Stavissky, E. A. Stumbur, and L. F. Sherman, Second Geneva Conf., Vol. 15, p. 50, paper P/2219 (1958). Measured ^{116}In decay. Relative to I (n,γ) σ.

R. L. Macklin, N. H. Lazar, and W. S. Lyon, Phys. Rev. 107, 504 (1957). [Oak Ridge]. Counted 1.28 MeV gamma following ^{116}In decay. Sb-Be source. Relative to I (n,γ) σ = 820 $\pm$ 60 mb.

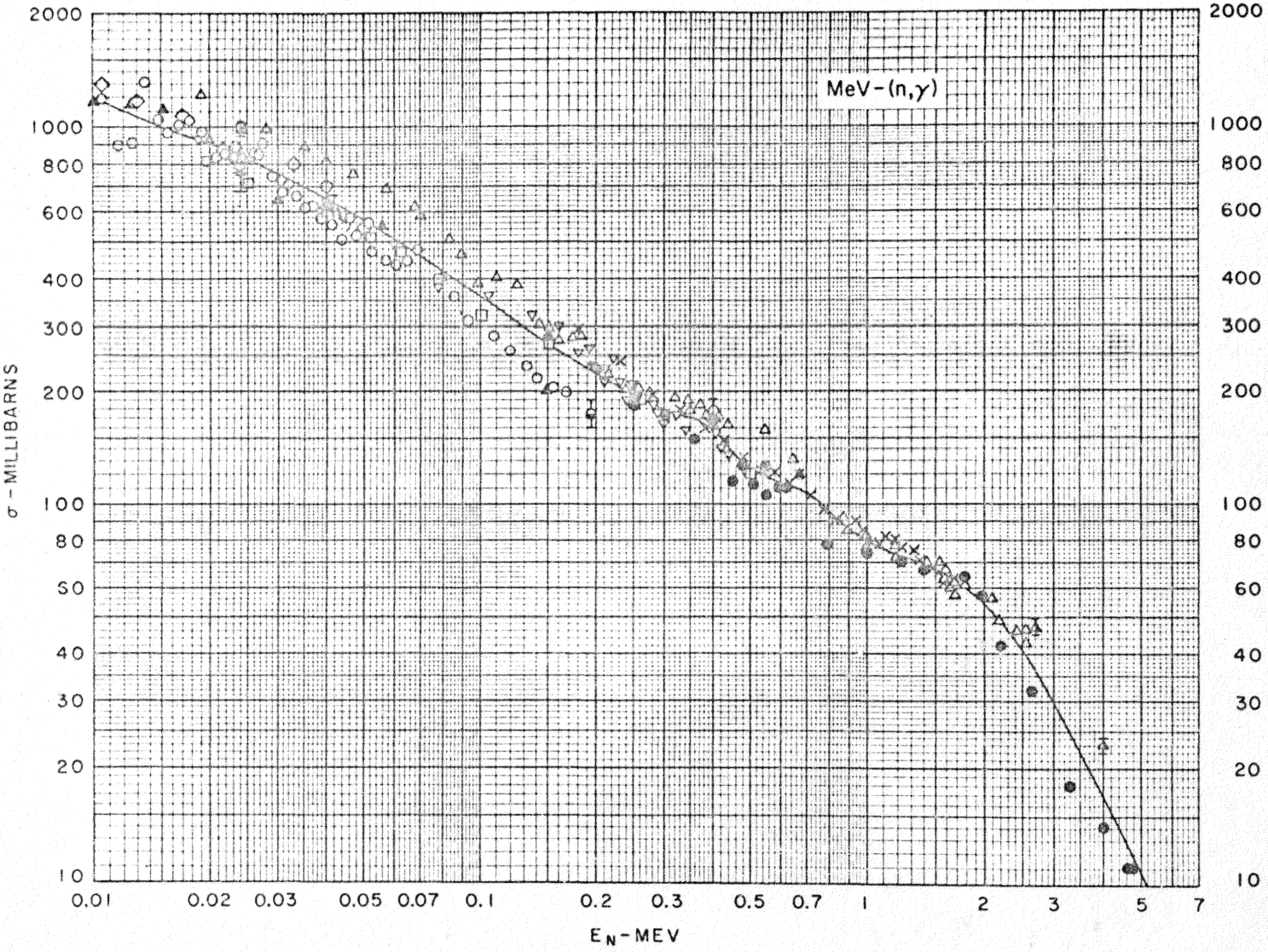

FIGURE 22. ^{127}I

^{127}I

▩ J. C. Robertson, Nuclear Phys. 71, 417 (1965). [Teddington, England]. Counted ^{128}I decay betas. Calibrated Sb-Be source.

X S. A. Cox, Phys. Rev. 133, B378 (1964). [Argonne]. Counted 450-keV gamma following ^{128}I decay. Relative to I thermal (n,γ) σ = 6.22 $\pm$ 1.5 b and ^{235}U σ_F. Renormalized here to ^{235}U σ_F curve in Vol. III, Reference 23.

◊ Yu. P. P. Popov and F. L. Shapiro, Zhur. Eksp. i Teoret. Fiz. 42, 988 (1962). [Lebedev Inst.]. [Transl. in Soviet Phys. - JETP 15, 683 (1962)]. Slowing-down-time spectrometer.

O J. H. Gibbons, R. L. Macklin, P. D. Miller, and J. H. Neiler, Phys. Rev. 122, 182 (1961). [Oak Ridge]. Large liquid scintillator tank. Relative to In (n,γ) σ.

Δ Yu. Ya. Stavisskii, V. A. Tolstikov, and V. N. Kononov, Atomnaya Energiya 10, 158 (1961). [Transl. in Soviet J. Atomic Energy 10, 153 (1961) and J. Nuclear Energy 16, 326 (1962)]. Counted ^{128}I decay betas. Relative to I thermal (n,γ) σ = 5.6 b and to ^{235}U σ_F. Renormalized here to I thermal (n,γ) σ = 6.2 b and to ^{235}U σ_F curve in Vol. III, Reference 23.

▲ L. W. Weston, K. K. Seth, E. G. Bilpuch, and H. W. Newson, Ann. Phys. 10, 477 (1960). [Duke]. Counted ^{128}I decay betas. Normalized to Mackin, et al. 57, below, at 24 keV.

+ H. W. Schmitt and C. W. Cook, Nuclear Phys. 20, 202 (1960). [Oak Ridge]. Sphere transmission measurement, Sb-Be source. [Value plotted is the corrected value as presented by H. W. Schmitt at the Neutron Flux Determination Symposium, Oxford, 1963. See EANDC-33 "U".]

◇ B. C. Diven, J. Terrell, and A. Hemmendinger, Phys. Rev. 120, 556 (1960). [Los Alamos]. Large liquid scintillator tank. Relative to ^{235}U capture + fission σ.

◪ T. S. Belanova, Atomnaya Energiya 8, 549 (1960). [Transl. in Soviet J. Atomic Energy 8, 462 (1961)]. Sphere transmission measurement. Sb-Be source. Corrected for multiple scattering.

◉ A. E. Johnsrud, M. G. Silbert, and H. H. Barschall, Phys. Rev. 116, 927 (1959). [Wisconsin]. Counted 450-keV gamma following ^{128}I decay. Relative to I thermal (n,γ) $\sigma = 5.6 \pm 0.3$ b and to ^{235}U σ_F. Renormalized here to I thermal (n,γ) $\sigma = 6.2$ b and to ^{235}U σ_F curve in Vol. III, Reference 23.

⊖ W. S. Lyon and R. L. Macklin, Phys. Rev. 114, 1619 (1959). [Oak Ridge]. Counted 450-keV gamma following ^{128}I decay. RdTh-D_2O source. Relative to ^{115}In (54 min) (n,γ) $\sigma = 195 \pm 10$ mb at 195 keV.

□ F. Gabbard, R. H. Davis, and T. W. Bonner, Phys. Rev. 114, 201 (1959). [Rice]. Counted ^{128}I decay betas.

▽ S. J. Bame, Jr., and R. L. Cubitt, Phys. Rev. 113, 256 (1954). [Los Alamos]. Counted ^{128}I decay betas and 26-keV K x-ray of ^{128}Te following ^{128}I decay. Relative to ^{235}U σ_F. Renormalized

here to ^{235}U σ_F curve in Vol. III, Reference 23.

A. I. Leipunsky, O. D. Kazachkovsky, G. Y. Artyukhov, A. I. Baryshnikov, T. S. Belanova, V. N. Galkov, Y. Y. Stavissky, A. E. Stumbur, and L. E. Sherman, Second Geneva Conf., Vol. 15, p. 50, Paper P/2219 (1958). Measured ^{128}I decay. Relative to ^{238}U σ_F.

R. L. Macklin, N. H. Lazar, and W. S. Lyon, Phys. Rev. 107, 504 (1957). [Oak Ridge]. Counted ^{128}I decay betas. Calibrated Sb-Be source.

(E_n < ~ 30 keV) as can be seen from an examination of Fig. 13. Above ~ 30 keV, in this example, the cross section is essentially parallel to the p-wave component. Hence, reliable values for S_o are dependent upon accurate values for the cross sections at low energies. Because of the spread of the neutron energy in this energy region, the shape of the cross section curve is least accurately known for E_n < 20 keV. Consequently, S_o can be expected to have large uncertainties. Reiterating, the error bars on the average resonance parameters determined in this experiment are only a measure of the uniqueness of the fit and do not reflect the large uncertainties in the energy.

The values for S_o are given in column 4 of the tables and can be seen to generally lie a good deal above other published values. They agree best, on the average, with Gibbons, et al.[9], who used a time-of-flight method and detected the prompt gammas emitted from the sample.

P-Wave Neutron Strength Functions, Column 5. Feshbach, et al.[37] predicted maxima in the p-wave strength function near atomic mass numbers 28, 90, and 216. Early measurements of $S_1 = \langle \Gamma_n^1 \rangle / \langle D \rangle$ by Barshall[38] and Newson[39] confirmed the existence of this giant resonance structure. However, p-wave neutron strength functions determined later[13,30] indicated a peak also near A = 110. This additional peak was attributed to the effect of a spin orbit coupling, and a satisfactory theoretical fit of the data has been generated by assuming an additional spin-orbit coupling term to the optical potential. An additional cause for the splitting or broadening of the p-wave

giant resonance near A = 100 has been suggested[46] as a spherical asymmetry of the highly excited states of the compound nucleus considered by the optical model theory.

By some combination of the above two phenomena there does appear to be a broadening of the p-wave giant resonance near A = 100. Even though the range of atomic numbers studied in the present work is small, a peak near A = 110 is indicated. There does seem to be a great discrepancy between the magnitudes of S_1 calculated from capture gamma measurements and those calculated from earlier activation and transmission methods. Gibbons'[9] work with capture gammas indicates values of S_1 differing by factors of two or three from other previous work. However, the results of the present work, using activation techniques, yield magnitudes of the order of those obtained by Gibbons. As far as is known, the present work is the first activation experiment giving values comparable to those of Gibbons. This is just an observation and is not meant to confirm or deny any previous results.

The values of the p-wave neutron strength functions calculated in this work are listed in column 5 of the tables and can be compared to those of previous experimenters.

Gamma-Ray Strength Functions, Column 3. As stated earlier, we have assumed that the γ-ray strength function, $\langle \Gamma_\gamma \rangle / \langle D_o \rangle$, is the same for s- and p-wave neutrons, resulting in a two-parameter fit for these functions.

The γ-ray strength function was determined to be the normalization factor necessary to make the experimental cross section curve coincide

with the resultant of the addition of the s- and p-wave components of the cross section. Hence, this parameter is dependent upon the magnitudes of the cross section, the s-wave component, and the p-wave component at the normalization energy of 24 keV. Values determined for $\sigma_{n\gamma}$ at 24 keV in this experiment are in general good agreement with previous results. However the overall shapes of the cross section curves do differ from those of other workers. This difference affects the value of S_o and S_1 and they in turn affect the magnitude of the γ-ray strength function. As before our values agree best with the values measured by Gibbons[9], and they lie below the values determined by other workers.

Column 3 of the tables contains the calculated magnitudes of the γ-ray strength functions measured in this work and values from several other workers.

NOTE. Table III contains two results for the average resonance parameters of natural Ag. The first row gives the values obtained by fitting the cross section curve in the method described in the analysis section. The second row gives values that one would expect to obtain by averaging the contributions of the two isotopes making up natural Ag.

Investigator	$\langle\Gamma_\gamma\rangle/\langle\Gamma_n^o\rangle$	$\langle\Gamma_\gamma\rangle/\langle\Gamma_n'\rangle$	$\{\langle\Gamma_\gamma\rangle/\langle D_o\rangle\}_s$ X 10^4	$S_o = \langle\Gamma_n^o\rangle/\langle D\rangle$ X 10^4	$S_1 = \langle\Gamma_n'\rangle/\langle D\rangle$ X 10^4
Present Work	20 ± 5	1.2 ± .1	7.9 ± 2.0	0.40 ± .14	6.58 ± 1.74
Furr(30) 3-parameter fit	64 ± 16	3.0 ± .9	26.3 ± 7.9	0.41 ± .14	2.3 ± .8
Furr(30) 2-parameter fit	48 ± 12	10 ± 2.5	17.6 ± 5.3	0.37 ± .11	1.8 ± .6
Weston, et al.(13)			25	0.5 ± .2	$2.6^{+1.9}_{-0.8}$
Pattenden(40)				0.35 ± .09	
Hughes, et al.(41)				0.5 ± .2	

Table I: ^{107}Ag Average Resonance Parameters

Investigator	$\langle\Gamma_\gamma\rangle/\langle\Gamma_n^o\rangle$	$\langle\Gamma_\gamma\rangle/\langle\Gamma_n'\rangle$	$\{\langle\Gamma_\gamma\rangle/\langle D_o\rangle\}_s$ X 10^4	$S_o = \langle\Gamma_n^o\rangle/\langle D\rangle$ X 10^4	$S_1 = \langle\Gamma_n'\rangle/\langle D\rangle$ X 10^4
Present Work	10^{+10}_{-8}	$0.4^{+.6}_{-.1}$	14.1 ± 1.85	$1.41^{+6}_{-.76}$	35.2^{+10}_{-20}
Furr (30) 3-Parameter Fit	48 ± 12	6 ± 2	23.6 ± 7.1	$0.49 \pm .17$	3.9 ± 1.4
Furr (30) 2-Parameter Fit	48 ± 12	6 ± 2	23.6 ± 7.1	$0.49 \pm .17$	3.9 ± 1.4
Weston, et al. (13)			19.8	$1.0 \pm .3$	3.3 ± 1.0
Pattenden (40)				$0.8 \pm .24$	
Chrien (42)				$0.76 \pm .27$	
Hughes, et al. (41)				$1.0 \pm .3$	

Table II. ^{109}Ag Average Resonance Parameters

Investigator	$\langle\Gamma_\gamma\rangle/\langle\Gamma_n^o\rangle$	$\langle\Gamma_\gamma\rangle/\langle\Gamma_n'\rangle$	$\{\langle\Gamma_\gamma\rangle/\langle D_o\rangle\}_s$ X 10^4	$S_o = \langle\Gamma_n^o\rangle/\langle D\rangle$ X 10^4	$S_1 = \langle\Gamma_n'\rangle/\langle D\rangle$ X 10^4
Present Work Visual Fit	4 ± 1.5	1.0 ± .2	11.3 ± 2.0	2.82 ± 1.17	11.3 ± 3.0
Present Work Isotopic Average	15 ± 7	$0.8^{+.35}_{-.10}$	11.3 ± 2.0	0.75 ± .37	$14.1^{+3.0}_{-6.7}$
Furr(30) 3-parameter fit	54 ± 14	5 ± 2	25.0 ± 7.5	0.46 ± .16	3.0 ± 1.1
Furr(30) 2-parameter fit	48 ± 12	8 ± 2.4	20.6 ± 6.2	0.43 ± .13	2.6 ± .9
Seth, et al.(43)				0.40 ± .10	2.5 ± .5
Desjardins, et al.(44)			20.3	0.51 ± .09	1.7 ± .8
Gibbons, et al.(9)			14.3	0.8	10 ± 3
Garg, et al.(45)				0.48 ± .04	
Weston, et al.(13)				0.53 ± .1	3.1 ± .4
Hughes, et al.(41)				0.30 ± .05	

Table III: Natural Ag Average Resonance Parameters

Investigator	$\langle\Gamma_\gamma\rangle/\langle\Gamma_n^0\rangle$	$\langle\Gamma_\gamma\rangle/\langle\Gamma_n'\rangle$	$\{\langle\Gamma_\gamma\rangle/\langle D_0\rangle\}_s$ X 10^4	$S_0=\langle\Gamma_n^0\rangle/\langle D\rangle$ X 10^4	$S_1=\langle\Gamma_n'\rangle/\langle D\rangle$ X 10^4
Present Work	$2^{+.2}_{-.5}$	0.3 ± .1	2.38 ± .36	$1.19^{+.35}_{-.22}$	7.93 ± 2.89
Furr(30) 3-parameter fit	32 ± 10	8 ± 4	7.2 ± 2.5	0.22 ± .09	0.9 ± .5
Furr(30) 2-parameter fit	32 ± 8	8 ± 4	7.2 ± 2.5	0.22 ± .09	0.9 ± .5
Seth, et al.(43)				0.20 ± .15	2.0 ± .5
Furr, et al.(5)	64 ± 16	1.5 ± .5		0.09 ± .03	3.9 ± 1.4
Gibbons, et al.(9)			3.9	0.5	8 ± 2
Weston, et al.(13)			6.0	0.31 ± .06	$2.0^{+2}_{-.8}$

Table IV: ^{115}In Average Resonance Parameters

Investigator	$\langle\Gamma_\gamma\rangle/\langle\Gamma_n^0\rangle$	$\langle\Gamma_\gamma\rangle/\langle\Gamma_n'\rangle$	$\{\langle\Gamma_\gamma\rangle/\langle D_0\rangle\}_s$ X 10^4	$S_0 = \langle\Gamma_n^0\rangle/\langle D\rangle$ X 10^4	$S_1 = \langle\Gamma_n'\rangle/\langle D\rangle$ X 10^4
Present Work	$1.0\ ^{+\ 3}_{-\ .5}$	1.0 ± .2	4.02 ± .25	$4.02\ ^{+\ 2.03}_{-\ 3.50}$	4.02 ± .84
Furr(30) 3-parameter fit	6.0 ± 1.5	8 ± 2.4		1.11 ± .39	0.83 ± .29
Furr(30) 2-parameter fit	6.0 ± 1.5	8 ± 2.4		1.11 ± .39	0.83 ± .29
Seth, et al.(43)				0.55 ± .20	1.30 ± .25
Furr, et al.(5)	16 ± 2	8 ± 2		0.42 ± .10	0.83 ± .20
Desjardins, et al.(44)			6.65	0.84	
Gibbons, et al.(9)			6.65	0.84	3 ± 1.5
Weston, et al.(13)					1.5 ± .75
Garg, et al.(45)				0.69 ± .08	
Hughes, et al.(41)				1.2 ± .4	

Table V: ^{127}I Average Resonance Parameters

CONCLUSION

It is encouraging to note that the cross sections at a particular energy obtained in this experiment agree with the best estimates determined from other investigations. However, the cross section curves obtained in this work tend to cross over the curves obtained by other workers, with different slopes. This difference in shape of the cross section versus energy curves between this experiment and those of other workers results in average resonance parameters which are still subject to conjecture. The primary difficulty encountered in the present work was doubt concerning the exact shape of the cross section curve for neutron energies < ~ 30 keV.

In regard to this probable source of error, several suggestions are made for future experiments. First, a more efficient β/γ detector should be incorporated so that one might use thinner LiF targets and narrower samples. Each of these changes would result in a smaller energy spread and a consequent lessening of the number of choices one now has in estimating the shape of the cross section curve in the lower energy region. It would also be advantageous to determine the distribution of the proton beam that strikes the LiF target. This could be done by sweeping the proton beam across a target having a narrow proton capture resonance and examining the γ-ray activity as the beam crosses the sample. One could then obtain information about the variations from the assumed symmetric distribution of protons in the beam. Once this distribution is obtained, care should be taken to assure that it does not become biased during the performance of the

actual experiment. (This bias could arise from the proton beam being collimated in a manner which remove more protons from one side of the distribution than the other.) To prevent such an occurence a set of two slits, one horizontal, one vertical, could be constructed as a collimator such that the current striking each half of the slits could be monitored at the operator console. With proper adjustments an operator could assure an unbiased proton beam by making certain that the current on the four plates remains equal or fixed relative to each other. Finally, it is suggested that a finer grid of energies be used in the 3-30 keV energy range. Even though the energy spread of adjacent points might overlap, this would provide more information as to the shape of the curve in this critical region.

With these improvements, the method of analysis described herein should be applicable for a large number of nuclides and should yield accurate values of the average resonance parameters.

BIBLIOGRAPHY

1. Greebler, A. and Hutchins, B. A., "User Requirements for Cross Sections in the Energy Range from 100 eV to 100 keV", Conference on Neutron Cross Section Technology, Book I, p. 357, Washington, D. C., (1966).

2. Bell, George I., "Cross Sections for Nucleosynthesis in Stars and Bombs", Conference on Neutron Cross Section Technology, Book I, p. 454, Washington, D. C., (1966).

3. Emmerich, W. S., "Optical Model Theory of Neutron Scattering and Reactions", Fast Neutron Physics, Vol. IV, Part II, p. 1057, Interscience Publishers, New York, (1963).

4. Schmitt, H. W. and Cook, C. W., Nuclear Physics, Vol. 20, p. 202, (1960).

5. Furr, A. Keith and Tucker, John R., "Average s- and p-wave Resonance Parameters of ^{115}In and ^{127}I", Nuclear Science and Engineering, Vol. 35, p. 364, (1969).

6. Newson, H. W. and Rohrer, R. H., "Shell Effects in Highly Excited Nuclei", Physical Review, Vol. 94, No. 3, p. 654, (1954).

7. Lindsay, James G., "Average Neutron Cross Section Measurements with Reactor Neutrons", Ph.D. Thesis, V.P.I., (pending).

8. Macklin, R. L. and Gibbons, J. H., "Capture-Cross-Section Studies for 30-220 keV Neutrons Using a New Technique", Phys. Rev. Vol. 159, No. 4, p. 1007, (1967).

9. Gibbons, J. H., Macklin, R. L., Miller, P. D., and Neiler, J. H., "Average Radiative Capture Cross Sections for 7- to 170 keV Neutrons", Phys. Rev., Vol. 122, No. 1, p. 182, (1961).

10. Diven, B. C., Terrell, J., and Hemmendinger, "Radiative Capture Cross Sections for Fast Neutrons", Phys. Rev., Vol. 120, No. 2, p. 556, (1960).

11. Block, R. C., Vonderlage, F. C., and Weston, L. W., "Neutron Radiative Capture Measurements", ORNL Report 3085, p. 48, (1961).

12. Bilpuch, E. G., and Weston, L. W., and Newson, H. W., "Neutron Capture Cross Sections in the keV Region, Part I", Annals of Physics, Vol. 10, p. 455, (1960).

13. Weston, L. W., Seth, K. K., Bilpuch, E. G., and Newson, H. W., "Neutron Capture Cross Sections in the keV Region, Part II", Annals of Physics, Vol. 10, p. 477, (1960).

14. Gibbons, J. H., "Neutron Cross Sections in the Energy Range 100 eV < E_n < 100 keV: Recent Progress, Current Status, Future Outlook", Conference on Neutron Cross Section Technology, Book 1, p. 404, Washington, D. C., (1966).

15. Marion, J. B., "Neutron Threshold Measurements", Progress in Fast Neutron Physics, p. 23, The University of Chicago Press, (1963).

16. Gibbons, J. H. and Newson, Henry W., "The $^7Li(p,n)^7Be$ Reaction", Fast Neutron Physics, Vol. IV, Part I, p. 133, Interscience Publishers, New York, (1963).

17. Breit, G. and Bloch, I., "Resonances in $^7Li(p,n)^7Be$", Phys. Rev., Vol. 74, p. 397, (1948).

18. Taschek, Richard and Hemmendinger, Arthur, "Reaction Constants for $^7Li(p,n)^7Be$", Phys. Rev., Vol. 74, p. 373, (1948).

19. White, P. H., "The Room-Scattered Background By a Neutron Source in a Laboratory with Concrete Walls", Nuclear Instruments and Methods, Vol. 39, p. 256, (1966).

20. Hughes, Donald J., Neutron Cross Sections, Pergamon Press, New York, pp. 54-58, (1957).

21. Winters, Ronald R., Half-Life Determination of Lutetium-176 by Three Coincidence Methods, Ph.D. Dissertation, VPI, p. 13, (1967).

22. Robertson, J. C., Nuclear Physics, Vol. 71, p. 417, (1965).

23. Neutron Cross Sections, Vol. II B, BNL 325, Second Edition, Supplement #2, Physics-TID-4500, (1966).

24. Stam, Ephraim, Performance Characteristics of the V.P.I. Training and Research Reactor (UTR-10), Masters Thesis, VPI, (1962).

25. Blatt, John M. and Weisskopf, Victor Z., Theoretical Nuclear Physics, John Wiley and Sons, New York, Chapter IX, (1952).

26. Breit, G., and Wigner, E., "Capture of Slow Neutrons," Phys. Rev. Vol. 49, p. 519, (1936).

27. Rae, E. R., Margolis, B., and Troubetzkoy, E. S., Phys. Rev., Vol. 112, p. 492, (1958).

28. Porter, C. E. and Thomas, R. G., Phys. Rev., Vol. 104, p. 483, (1956).

29. Stolovy, A. and Harvey, J. A., Phys. Rev., Vol. 108, p. 353, (1957).

30. Furr, A. Keith, Average Resonance Parameters Near A = 100, Ph.D. Dissertation, Duke University, (1962).

31. Asghar, M., Moxon, M. C., and Chaffey, C. M., Conference on the Study of Nuclear Structure with Neutrons, Antwerp, Paper 65, (1965).

32. Rae, E. R., Collins, E. R., Kinsey, B. B., Lynn, J. E., and Wiblin, E. R., Nuclear Physics, Vol. 5, p. 89, (1958).

33. Belanova, T. S., Van'kov, A. A., Mikhailus, F. F., and Stavisska, Yu. Ya., Atomnaya Energiya, Vol. 19, p. 3, (1965).

34. Isakov, A. I., Popov, Yu. P., and Shapiro, F. L., Soviet Physics-JETP, Vol. II, p. 712, (1960).

35. Popov, Yu. P. and Shapiro, F. L., Soviet Physics-JETP, Vol. 15, p. 683 (1962).

36. Lane, A. M. and Lynn, J. E., Nuclear Physics, Vol. 17, p. 563, (1960).

37. Feshbach, H., Porter, C. E., and Weisskopf, V. E., Phys. Rev., Vol. 96, p. 448, (1954).

38. Barshall, H. H., Phys. Rev., Vol. 86, p. 431, (1952).

39. Newson, H. W., Block, R. C., Nichols, P. F., Taylor, A., and Furr, A. K., Annals of Physics, Vol. 8, p. 211, (1959).

40. Pattenden, N. J., Proceedings of the International Conference on the Study of Nuclear Structure with Neutrons, Paper 92, p. 532, (1965).

41. Hughes, D. J., Zimmerman, R. L., and Chrien, R. E., Phys. Rev. Letters, Vol. 1, p. 461, (1958).

42. Chrien, R. E., Phys. Rev., Vol. 141, p. 1129, (1966).

43. Seth, K. K., Tabony, R. H., Bilpuch, E. G., and Newson, H. W., Physics Letters, Vol. 13, p. 70, (1964).

44. Desjardins, J. S., Rosen, J. L., Havens, W. W., and Rainwater, J., Phys. Rev., Vol. 120, p. 2214, (1960).

45. Garg, J. B., Rainwater, J., Havens, W. W., Phys. Rev., Vol. 137, p. B547, (1965).

46. Perey, F. G. J., Bull. Am. Phys. Soc., Series II, Vol. 7, p. 58, (1962).

The vita has been removed from the scanned document

CAPTURE CROSS SECTIONS IN THE KEV REGION

Wayne Wesley Campbell

ABSTRACT

Many workers have attempted to determine neutron absorption cross sections and average resonance parameters with varying degrees of success. Values of the latter parameters for a given isotope often vary as much as a factor of two or three from one worker to another. This dissertation is an attempt to remove some of this uncertainty.

Natural silver and the isotopes ^{107}Ag, ^{109}Ag, ^{115}In, and ^{127}I have been irradiated by the monoenergetic neutrons emitted at 90^{o} to a proton beam striking a ^{7}Li target. These samples were then counted for their β and γ activity and their absolute cross sections relative to the cross section of ^{127}I at 24 keV were calculated over the energy range of from 3 to 155 keV. These measured cross section versus energy curves were used to determine the γ-ray strength functions, $\langle \Gamma_{\gamma} \rangle / \langle D_{o} \rangle$, the s-wave neutron strength functions, $\langle \Gamma_{n}^{0} \rangle / \langle D \rangle$, and the p-wave neutron strength functions, $\langle \Gamma_{n}^{1} \rangle / \langle D \rangle$. Because of data limitations it has been assumed that the γ-ray strength function is the same for both s- and p-wave neutrons.

The cross sections determined are in general good agreement with the values previously reported but differ somewhat in shape. This shape variance results in values for the average resonance parameters which are somewhat higher than values reported by other workers.